Glacier surge monitoring from temporally dense elevation time series: application to an ASTER dataset over the Karakoram region

Luc Beraud¹, Fanny Brun¹, Amaury Dehecq¹, Romain Hugonnet², and Prashant Shekhar³

Correspondence: Luc Beraud (luc.beraud@univ-grenoble-alpes.fr, luc.beraud@protonmail.com)

Abstract.

Glacier surges are spectacular events that lead to surface elevation changes of tens of meter metres in a period of a few months to a few years, with different patterns of mass transport. Existing methods of elevation change estimate of to derive elevation change associated with surges, and subsequent quantification of their mass transported the transported mass, rely on differencing pairs of digital elevation models (DEMs) that are not may not be acquired regularly in time. More and more long time series of elevation data are becoming available. In this study, we propose a workflow to filter and interpolate a dense time series of DEMs specifically for the study of surge events. We test this workflow on a global 20-year dataset of DEMs from the optical satellite sensor ASTER. The multi-steps Advanced Spaceborne Thermal Emission and Reflection Radiometer (ASTER). The multistep procedure includes linear non-parametric Locally Weighted Regression and Smoothing Scatterplots (LOWESS) filtering and Approximation by Localized Penalized Splines (ALPS) interpolation. We run the workflow over the Karakoram mountain range (High Mountain Asia). We compare the produced dataset to previous studies for four selected surge events, on Hispar, Khurdopin, Kyagar and Yazghil glaciers. We demonstrate that our workflow captures thickness changes at on a monthly scale with detailed patterns of mass transportation. Such patterns includes include surge front propagation—and changes in dynamic balance line, and slow surge onset among others, and allows an unprecedentedly among others. Our results allow a remarkably detailed description of glacier surges at the scale of a large region. The workflow preserves most of the elevation change signal, with underestimation or smoothing in a limited number of surge cases.

1 Introduction

Surge events are extreme cases of the continuous spectrum of glacier flow instabilities (Herreid and Truffer, 2016). Surges are quasi-periodic events characterised by an characterized by abnormally rapid glacier flow, lasting from several months to years (Cuffey and Paterson, 2010). (Bhambri et al., 2017; Cuffey and Paterson, 2010). Large masses of ice are transported during surge events, causing important thickness changes (Bhambri et al., 2017, 2022). They occur on a limited number of glaciers , called known as surge-type glaciers. They, which are clustered in a few parts regions of the globe, among which is Karakoram, the Karakoram in High Mountain Asia (Sevestre and Benn, 2015) (Guillet et al., 2022; Sevestre and Benn, 2015).

¹Université Grenoble Alpes, CNRS, IRD, Grenoble INP, INRAE, Institut des Géosciences de l'Environnement (IGE), 38000 Grenoble. France

²University of Washington, Civil and Environmental Engineering, Seattle, WA, USA

³Embry-Riddle Aeronautical University, Daytona Beach Campus, FL, USA

Surges can occur on both land-terminating and tidewater glaciers, and on either polythermal or temperate glaciers (Cuffey and Paterson, 2010). The mechanisms behind the surge phenomenon (reasons for being surge-typeorigin, surge trigger, etc.) are still not fully understood (Benn et al., 2023; Terleth et al., 2021; Thøgersen et al., 2024; Crompton et al., 2018), not yet fully understood, and this subject continues to be the subjects of developments and theories (e.g., Benn et al., 2023; Crompton et al., 2018; Terlet Surge events are often studied a posteriori with remote sensing data. Satellite imagery is used for visual mapping, to derive surface velocity maps or elevation (Paul et al., 2022). Remote sensing data have been used in numerous studies, ranging from the inventorying of surge-type glaciers to detailed case studies (e.g., Guo et al., 2020; Round et al., 2017; Guillet et al., 2022; Bhambri et al .A large number of studies used surface velocities derived from optical and radar satellites to estimate precise surge dates and evolution patterns (e.g., velocities over 2-3 weeks in Round et al. (2017), Guo et al. (2020)...). Surface velocities are also used in combination with other data, such as elevation change data, to map surge-type glacier in inventories (Guillet et al., 2022; Guo et al., 2022 The variations of the glacier surface elevation is a major key of observation for this field of study. The study of elevation changes 35 over time can give some insight into the current state of a glacier in its surge cycle. It permits to compute the volume of ice transferred during a surge event, along with the spatial extent affected (e.g., Bhambri et al., 2022; Gao et al., 2024; Steiner et al., 2018) . A few surge-type glaciers may begin surging after a critical mass has built up in the reservoir; an information that is accessible with elevation differencing (Kotlyakov et al., 2018; Lovell et al., 2018). Elevation data, and by extension surface slope, can be used to compute and analyse basal shear stress, which may play a critical role in the triggering of surges (Beaud et al., 2022; Thøgersen et al., 2024). Remote sensing analysis from satellite imagery permits to generate various products for the study of surges (Paul et al., 2022). Among them, digital elevation models (DEMs) can be produced at local to global scale, providing observations of the elevation of the glacier surface and its variation along time (e.g., Hugonnet et al., 2021). Such data have been used in numerous studies, ranging from the inventorying of surge-type glaciers to detailed case studies (e.g., Bhambri et al., 2022; Guillet et al., 2022; Guo et al., 2020; Round et al., 2017). However, the use of DEMs for the study of surges is often limited to a few dates or specific case studies. Surges are short-term events with important elevation changes, and surge-type elevation time series are non-linear. The retrieval of mass transfer variations happening during single surge events requires dense elevation time series with a resolution of one or a few months in principle. Temporally dense elevation time series from satellites covering a long period of time have recently become available for studying glacier elevation change. Such acquisitions started around the year 2000, with time series now spanning more than two decades, long enough to capture 50 entirely a number of surge events. Elevation measurements from altimetry mission (laser or radar) benefits from good temporal resolutions, such as ICESat-2, CryoSat-2 etc.) benefit from a good temporal resolution, but their spatial resolution and coverage does not permits to study surge events effectively (e.g., Wang et al., 2021; Yue et al., 2023; Lai and Wang, 2022). The use of suitable digital elevation models (DEMs) for the study of surges is often limited to a few dates or specific case studies sparsity 55 prevents most spatial analysis (e.g., extent, propagation) as opposed to high resolution DEMs (e.g., Wang et al., 2021; Yue et al., 2023; Lai . Several studies use SAR dense have used dense SAR time series on surge case studies, usually without time series filtering technique (Round et al., 2017; Wendt et al., 2017; Zhang et al., 2023). Dense elevation time series have been used

in studies of from optical sensors have been successfully used to study long-term elevation trends and multi-year glacier

mass balance (e.g., Brun et al., 2017; Shean et al., 2020; Hugonnet et al., 2021). However, surges are short-term events with important elevation changes, and surge-type elevation time series are non-linear. The retrieval of mass transfer variations happening during single surge events requires dense elevation time series with a weekly or monthly resolution in principle. However, stereo satellite sensors with systematic acquisitions worldwide and with a high temporal resolution have rather coarse resolutions (> 10 m)(e.g., Brun et al., 2017; Hugonnet et al., 2021; Shean et al., 2020). The TERRA satellite with its ASTER sensor is the only optical stereo mission that provides systematic and global acquisitions, but it has a spatial resolution of 15 m (Berthier et al., 2023). The DEMs derived from these sensors have elevation precisions of similar magnitude and sometime large noises. They need techniques of filtering sometimes large artefacts (e.g., cloud sensitivity, jitter, lack of stereo correlation on saturated/textureless terrain...). Noisy DEMs require specific filtering techniques that preserve surge signals (i.e., preserve elevation observations before, during and after the surge). Basic thresholds and linear methods might misinterpret surge observations as outliers. Also, the volume transported or slope should be computed at consistent dates across a whole glacier. Thus, a final step of interpolation is required. Various approaches have been implemented in the context of glacier elevation time series analysis. A recent study has exploited a Bayesian framework by inference applied to elevation change to filter outliers, which requires prior knowledge from diverse sources (Guillet and Bolch, 2023). It has been tested on surge-type glaciers, and it applies equally to dense time series. Hugonnet et al. (2021) have implemented a complex workflow for ASTER elevation time series over glaciers at global scale. It captures limited a number of non-linear elevation change, but fails to accurately reflect sudden changes associated with surge events. In Hugonnet et al. (2021) filtering and interpolation methods involve Gaussian Process Regression, based on a multi-term kernel defined by the variance of non-surge-type elevation changes. It results in a dataset where the elevation change of surge-type glaciers is underestimated, elevation changes retrieved at global scale. Shekhar et al. (2021) developed a spline-based approximation framework to model elevation changes with heterogeneous data, that can also be used for filtering. Another approach from Wang and Kääb (2015) not applied to surges is from Wang and Kääb (2015): it detects outliers, when no reference elevation exists, with a RANSAC (RANdom SAmple Consensus) algorithm. Other methods exist for the processing of time series of glacier surface velocity. Charrier et al. (2022) invert velocities using temporal closure of the displacement. Local regressions can be used with equivalent applicability for elevation, such as linear Linear non-parametric local regression regressions (LOWESS) that has have been used for non-surge glacier surface velocities (Derkacheva et al., 2020) and are suitable for elevation data. Existing procedures have different abilities and specific requirements to work properly with available DEM datasets from stereo imagery for the study of surges. To accurately estimate the parameters of surge events, existing methods must be adapted into a workflow that can process regional outlier-prone, moderate-precision, high-temporal-resolution DEMs and produce a temporally consistent dataset of elevation changes.

In this study, we present a workflow designed to filter and interpolate elevation time series of high temporal resolution during aim at developing a workflow to analyse outlier-prone, moderate-precision and high-temporal-resolution elevation dataset adapted to the specificity of surge events. We apply it to an unfiltered ASTER DEM dataset from Hugonnet et al. (2021). We use algorithms from the literature use established algorithms to filter outliers and interpolate elevations at monthly scale. We while preserving surge elevation signals. We apply it to an ASTER DEM dataset from Hugonnet et al. (2021). We produce a

regional dataset in the Karakoram region covering more than 100 surge-type glaciers. We assess the workflow performances, and we compare the outcome evaluate the performance of the workflow compared to the results of Hugonnet et al. (2021). We also compare the surge characteristics such as volumes transferred to other products and studies.

2 Data

125

In this study, we focus on the Karakoram region (Fig. 1). We use two existing surge-type glacier inventories that cover at least the period 2020 to 2020 2000 to 2018 in this region (Guillet et al., 2022; Guo et al., 2022). According to Guo et al. (2022), which considers glaciers larger than 0.4 km², there are 354 surge-type glaciers (individualizing with individualized tributaries) in the Karakoram and 128 probable or possible ones, representing about 8.6approximately 8.6% of the regional number of glaciers (39.5% in term-terms of area). Guillet et al. (2022) identified 223 surge-type glaciers on among glaciers larger than 5 km² (not individualizing tributaries). These studies show indicate that surge-type glaciers represents represent 39% to 45% of the glacierized area in this the Karakoram region.

We use the DEMs produced in the global study of Hugonnet et al. (2021), which ranged from 07/2000 to 09/2019 in this 105 region the Karakoram. They are generated from satellite images of the Advanced Spaceborne Thermal Emission and Reflection Radiometer (ASTER) sensor. They ASTER sensor. The DEMs have been processed at 30 m resolution with the MMASTER workflow, running under the open-source photogrammetric library MicMac (Girod et al., 2017; Rupnik et al., 2017). They are stacked in time on the same spatial grid, and we use the "Elevation time stack" product at All DEMs have been reprojected 110 to 100 m spatial resolution (see Extended Data Fig. 1, Hugonnet et al. (2021)). All DEMs with a root-mean-square-error of the elevation difference with and co-registered to the TanDEM-X on ice-free terrain above 20 m have been removed (Hugonnet et al., 2021; Rizzoli et al., 2017) global DEM (Rizzoli et al., 2017). We use all ASTER elevations produced estimated by MicMac for any stereo-correlation score, with lower correlation being associated to associated with higher uncertainty (Hugonnet et al., 2021). As an exception, we identify erroneous correlation scores of exactly 51%, likely due to a processing peculiarity in MicMac to compute this score, and remove their associated elevations for the rest of Finally, we apply a 115 preprocessing step specific to this dataset: 1) we filter pixels with a difference of more than 400 m between the ASTER DEM and the analysis. Each stack extends over a 1x1 degree tile and is coregistered over TanDEM-X DEM. Each DEM is generated from three consecutive ASTER granules and co-registered independently. The sliding of granules processing regularly results in several DEMs per date. The temporal sampling is heterogeneous-GLO-90 reference DEM 2) we merge the same-date 180 120 km DEM strips generated by Hugonnet et al. (2021) by keeping, in each pixel, the elevation with the highest correlation score.

The sampling is not regular in time and space, and parts of the mountain range have about twice as many DEMs as others (Fig. 1). Overall, 50% of consecutive on-glacier elevations are below 50 days apart, and about 90% are less than nine months apart. Said differently, 40% (7530% (62%, respectively) of the dates in the time series periods are between unfiltered observations which are less than six month months apart (a year, respectively) (Fig. 2, solid orange line).

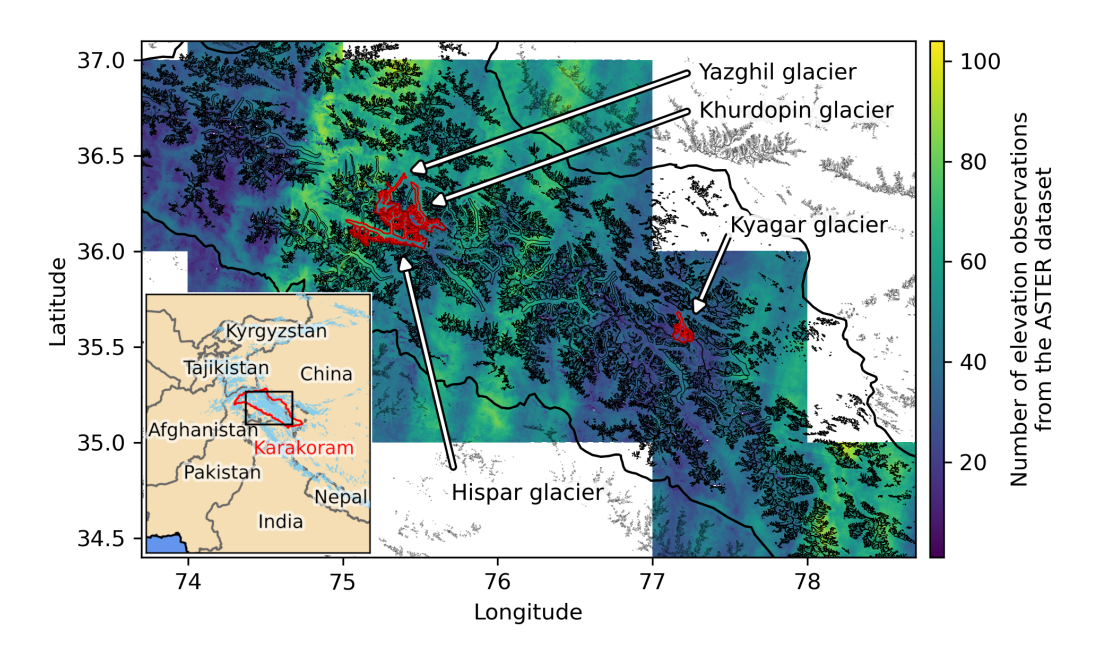


Figure 1. Study Map of the study area over in the Karakoram, with regional location indicated in the inset map. The colour scale shows the number of pre-filtered pre-processed ASTER-derived elevation observations over the period 2000-2019 from Hugonnet et al. (2021). (2021). Glacier outlines from RGI7.0 are shown in dark tonesblack. Glaciers The glaciers with the surge events analysed in section 4 and 5 are outlined in redare, from West to East: Hispar, Yazghil, Khurdopin and Kyagar glaciers.

We use the Copernicus DEM GLO-90 (European Space Agency and Airbus, 2022) as a reference elevation (European Space Agency and for coarse filtering of very large outliers. It is edited from the data of the TanDEM-X mission between 2011 and 2015. The impact of radar penetration is negligible compared to the threshold used (hundreds of metres).

130 3 Methods

3.1 General workflow

We aim to develop a workflow to filter and interpolate stacks of ASTER DEMs, specifically designed to handle surge events. We use the workflow of Hugonnet et al. (2021) as a baseline to which we compare our own workflow. It is noteworthy should be noted that Hugonnet et al. (2021) handled the same ASTER DEMs, but it (without our pre-processing step), but was not specifically designed for surge type surge-type glacier elevation changes. Our workflow is divided into three main sections two main steps (Fig. 3).

First, we implement pre-filtering steps. Second, we filter the dataset to remove remaining outliers . Third, we interpolate elevation along time. More precisely, our workflow follow the stepsdescribed on Fig. 3in three steps:

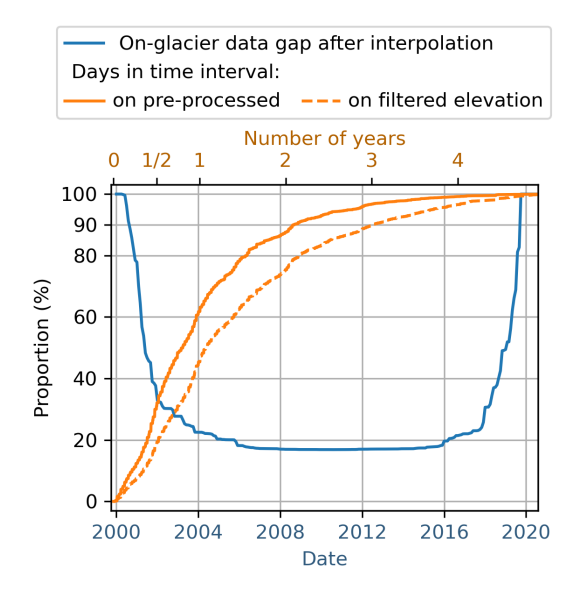


Figure 2. Data gap and temporal coverage of the time series at different processing level. In blue, the proportion of the <u>interpolated</u> on-glacier data gap <u>per dateover the time series period</u>, <u>before and</u> after the processing workflow. In orange, the proportion of days that fall below the time interval range (e.g., <u>nearly 7562</u>% of any date in the time series periods are between <u>unfiltered pre-processed</u> observations less than a year apart). The x-axis are independent, the y-axis is shared.

- 1. Spatial filter: we filter out pixels with a difference of more than 400 m between the ASTER DEM and GLO-90 reference DEM.
 - 2. Merging of strips: we merge the DEM strips on the same day by keeping, at the pixel level, the elevation with the highest correlation score at overlaps.
 - 3. LOWESS workflow, core step of the filtering: we apply a LOWESS workflow (detailed in subsection 3.2)to further filter pixels that are not consistent with other temporally close observations in the time series.
- 4. Morphological 3x3 erosion: we implement a morphological erosion with a 3x3 kernel on the binary data mask. The ASTER elevation errors of this dataset are often correlated spatially to their neighbours. Removing the pixels directly around data gaps removes further outliers. It removes pixels adjacent to outliers, as they also have reduced precision due to the photogrammetric processing.
 - 5. Removal of time series with less than 10 points: we consider such time series not dense enough for our application.
- 6. Regular temporal interpolation with ALPS-REML:

Second and finally, we interpolate the time series with at regular time intervals using a B-spline method with which includes an automatic hyperparametrisation. We develop it algorithm (ALPS-REML), detailed in subsection 3.3. The interpolated elevations are provided as a monthly time series.

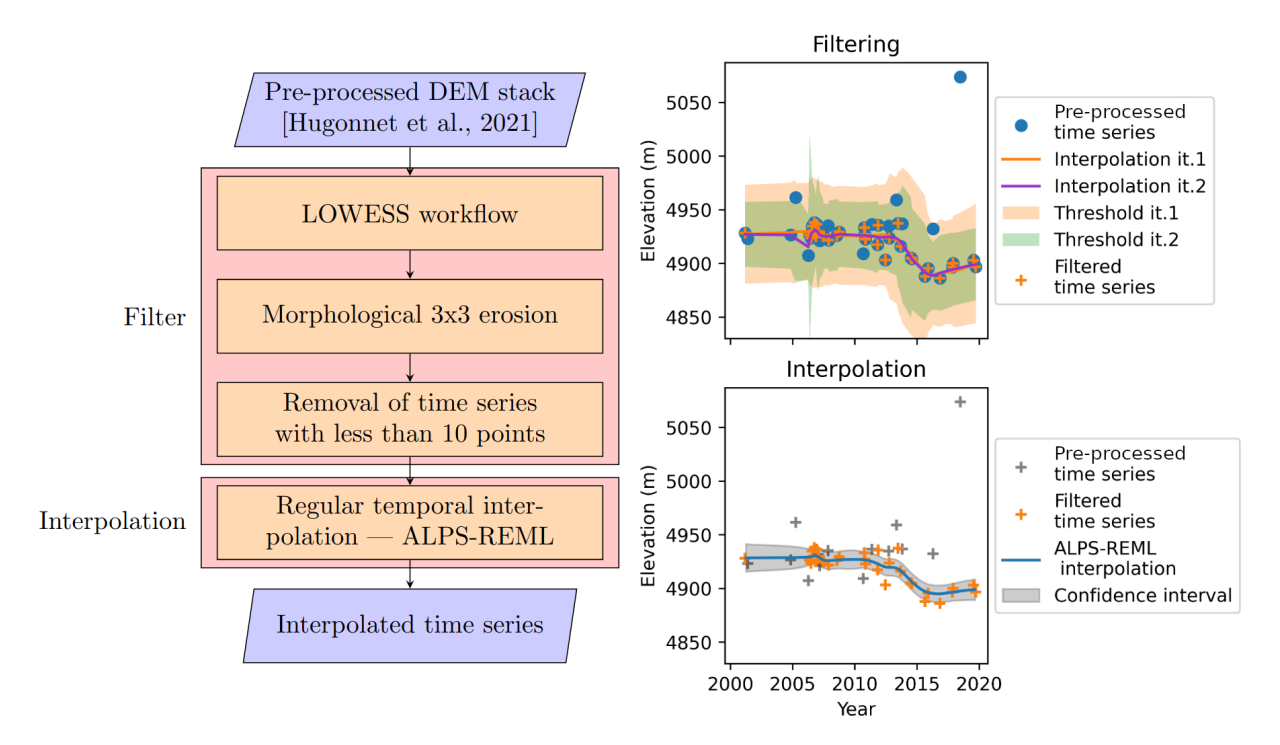


Figure 3. The complete workflow Workflow of the elevation time series processing, with an example of time series processed. Abbreviations: "it." ~in the time series legend stands for iteration —(of the LOWESS algorithm). The location of the time series exemplified is labelled "TSTSa" ~in the caption and map of Fig. 7.c. A version of the filtering of the time series, coloured by the elevation error estimate, is provided in Supplementary Fig. S8.

3.2 LOWESS filter

- The pre-filtering step is very coarse and excludes only the largest outliers. We thus additionally We filter the elevation time series using the Locally Weighted Regression and Smoothing Scatterplots (LOWESS) LOWESS algorithm in a sequence detailed later (Cleveland and Devlin, 1988; Derkacheva et al., 2020). It is a non-parametric, moving weighted regression. We use the Python *scikit-misc* implementation. For our dataset, the output of the regression is to too sensitive to noise overall and too smooth over surges to be used directly as an interpolation of the elevation, so we use it for filtering only.
- 160 Here are the main parameters that have been tuned manually (Fig. 4):
 - span: it is the Span: smoothing parameter, expressed as the fraction [0-1] of points of the time series used at each local regression. A larger value implies more smoothing. We set it at 0.4 and 0.3 for the two iterations, respectively.
 - degree Degree: degree of the local polynomial regression. We choose a degree 2.
 - family Family: assumed distribution of the errors, with a choice between "gaussian" (fit is performed with a least-squares) and "symmetric" (fit is performed robustly by redescending M-estimators). We use "symmetric".

- weights Weights: weights to be given to individual observations in the sum of squared residuals. We use the uncertainty provided for each elevation in Hugonnet et al. (2021), which models heteroscedasticity (variable error) as a function of slope and the quality of stereo-correlation based on elevation differences on stable terrain (Hugonnet et al., 2022).

We use the LOWESS algorithm in the following sequence (Fig. 5): we run two iterations of the LOWESS regression with a decreasing smoothing factor. At each iteration, we compute a threshold envelope around the regression which is used to remove points falling outside of it. The envelopes are derivative-varying to prevent the filtering from removing true filter from removing accurate observed signals close to surge events. For the two consecutive iterations of outlier removal, respectively (plot in Fig. 5): the thresholdto the regression ranges from 30 m width (resp. 45 m) at 0 m. We assume fast-varying elevation (high derivative) is a potential surge, and then use a larger threshold. For the first iteration, the threshold is 150 m for fast-varying elevation above 50 m yr⁻¹ derivative(constant elevation) to and then linearly down to 45 m at lower elevation change rate. The threshold is lower for the second iteration: 100 m (resp. 150 m) at above 50 m yr⁻¹ derivative (assumed to be a potential surge signal). The worst elevation change rate, down to 30 m below. The worse time series have large temporal data gaps which can create computational errors for small smoothing parameters. Therefore, at each regression, we implement a step-by-step increase in the smoothing parameter in case of such errors, depicted as the faction value in Fig. 5. In case of computational error remaining after a +0.05 (resp. +0.10) increase of the fraction parameter, we filter out the full time series.

3.3 ALPS - REML interpolation

185

190

ALPS or Approximation by Localized Penalized Splines is a unified time series modeling modelling framework introduced in Shekhar et al. (2021). ALPS builds on the localized nature of B-spline basis functions to model time series with highly non-uniform sampling, thereby improving the state of the art in this domain. In this research, we use a mixed modeling analog modelling analogue of the statistical B-spline regression model introduced in Shekhar et al. (2021). This is motivated from by the capability of the mixed models to segregate high frequency and low frequency—high-frequency and low-frequency components of the overall model, thus allowing us to narrow down the effect of the regularization/smoothing specifically on the high frequency—high-frequency components that drive the overfitting behavior-over-fitting behaviour.

Another change inherent in our approach, as compared to the approach described in Shekhar et al. (2021), is the model fitting algorithm. As described in Shekhar et al. (2021), the original ALPS model used the Generalized Cross Validation (GCV) metric for estimating the model parameters. However, here we take an alternative route and use the restricted maximum likelihood (REML) approach for fitting our model. Just to give a little background, GCV metric quantifies the generalization error of model by predicting at data points, not used for fitting the regression model. And hence, Hence, the minimization of GCV metric forces the model to predict accurately at unseen locations as described in Wahba (1990). REML on the other hand formulates the problem from a statistical perspective and optimizes the regression parameters such so that the probability of observing the data is maximized. A more detailed explaination explanation of REML can be found in Ruppert et al. (2009). The reason for choosing REML over GCV in this work can be attributed to the fact that GCV is well known to under-estimate underestimate model uncertainty, thereby providing over-confident prediction predictions which in some extreme cases can be

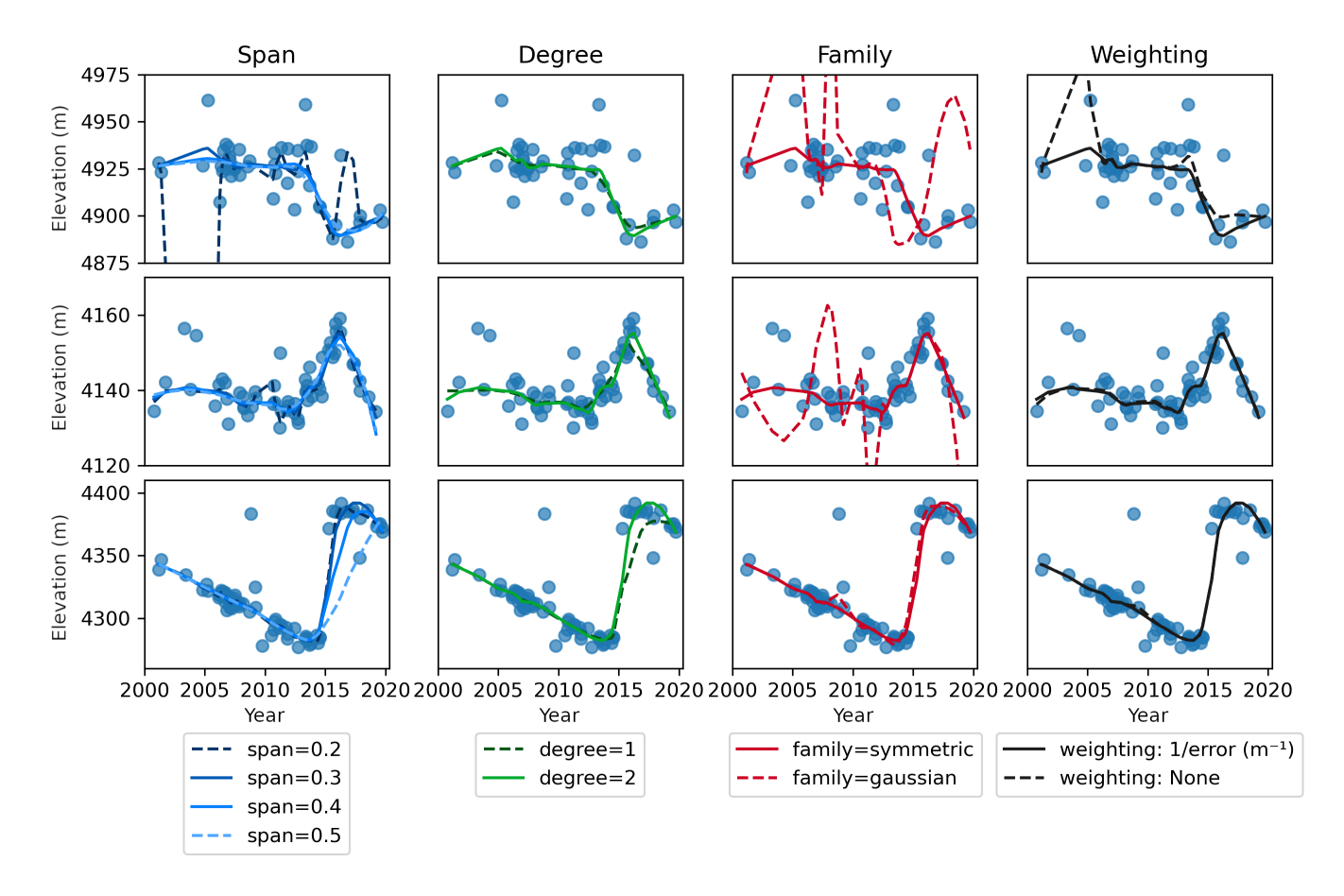


Figure 4. Impacts of the different LOWESS parameters on the filtered time series. Each column corresponds to the different LOWESS results for different values of each of the four main parameter. Plain lines are the final selected values. The line corresponds to three different data points (TSa-c in the line order, locations shown on Fig. 7.c).

misleading. Additionally, for the time series under consideration in this work, the ALPS model with the original GCV based model fitting was overfitting to noise, making it unsuitable. In order to produce interpolated results in this paper, we use the same ALPS-REML code. Wehowever, however, set a degree of the basis functions p of 4, and an order of penalty q of 1.

We compare extensively Gaussian Process Regression (GPregression) and ALPS-REML in our study. GP-

3.4 Gaussian Process regression

Gaussian Process (GP) regression is a non-parametric method, for which we can define a kernel with mathematical functions that fit the prior belief of the phenomenon to model (e. g., periodicity, linear trend. ..). that relies on estimating the data covariance to provide an optimized interpolator (Cressie, 1993; Rasmussen and Williams, 2005; Williams, 2007). Under certain

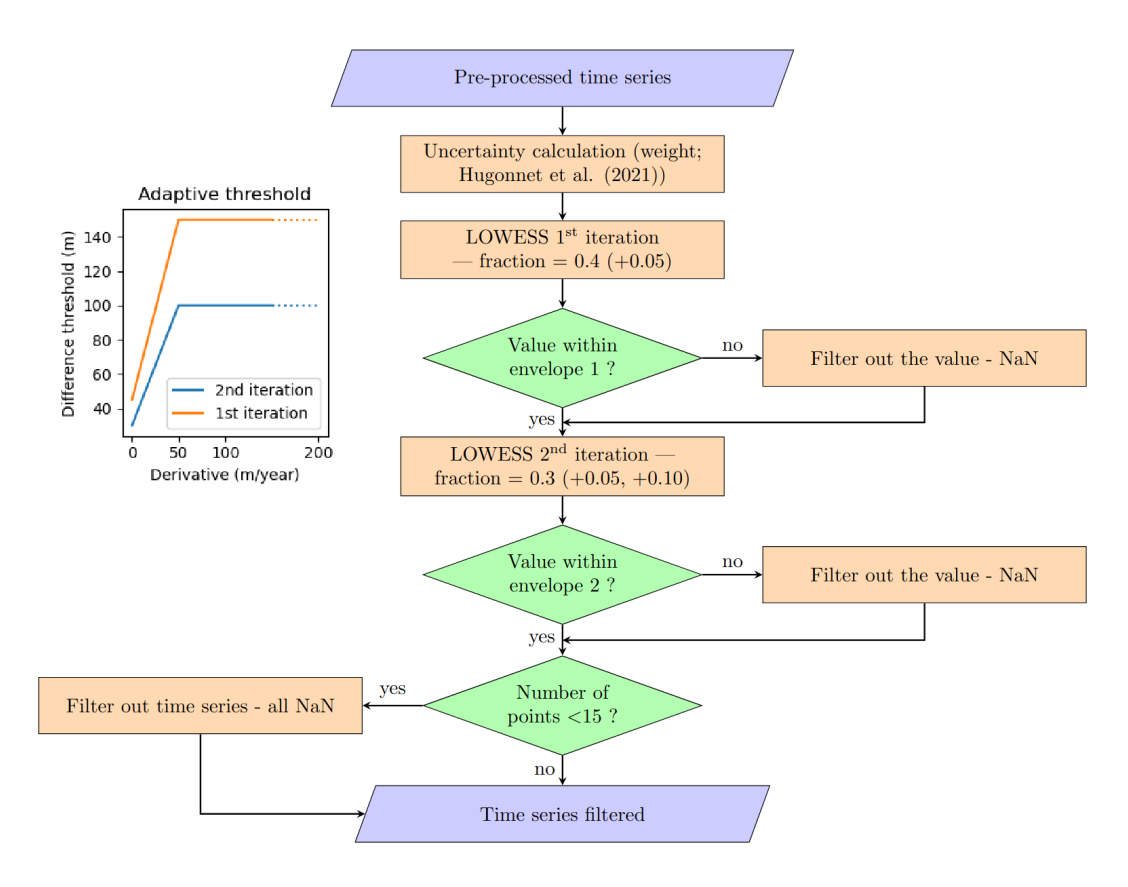


Figure 5. Complete workflow of the LOWESS filter step. The envelopes are the maximum distance threshold allowed between the LOWESS regression and the time series values, which vary with the LOWESS regression derivatives as shown in the inserted plot on the top-left.

assumptions, including notably second-order stationarity, GP regression has been shown to be the "best linear unbiased predictor". It is the method used by Hugonnet et al. (2021) on this same dataset, to compute long-term mass balance estimations worldwide. GP regression is more complex to use, as it requires the definition of kernels based on variance analysis of the elevation changes. We use a GP covariance with terms estimated in Hugonnet et al. (2021) through a global variogram analysis. This analysis identified several kernel components (periodic, local, linear, etc.), that are not specifically tuned for surges.

210

We note that, contrary to GP regression, ALPS approximates the data with polynomials under the assumption of a degree of smoothness of the data, with no need for us to inform the behaviour of the data. Although both GP regression and ALPS need domain knowledge to decide the covariance kernel and spline degree/penalty respectively, from a user's perspective using GPs can be more complex owing to the well studied difficulty of optimizing the kernel, mean function and dimensionality (Pu, 2024). For ALPS on the opposite approximate the data with polynomials, which does not relies on prior belief of the data other hand, we simply manually select degrees and penalty orders from a small set of choices.

Reparametrization of the kernel used by Hugonnet et al. (2021) gave slightly worse results than those obtained with the ALPS-REML method. Our limitation with GP regression lies in the kernel definition which is done according to the variance of elevation changes. Each surge event is different in variances, which is also very different from the data variance in quiescent periods or on non-surge-type glaciers. We tried different settings of the kernels, that differ from the study of Hugonnet et al. (2021). We removed the seasonal term of the model. The length scale and the magnitude parameters of the remaining terms were manually tuned after testing. We added radial basis function terms of length scales of a few months and with a variance of a few tens/hundreds of square meters. The kernels that provided a suitable interpolation were slightly outperformed by the ALPS-REML algorithm. This could be reevaluated for other datasets (for e.g. less noisy), more complex steps or adapted GP regression processes and future advances (e.g., de-trending before GP regression or using other predictors).

3.5 Volume transfer estimate

250

We estimate the volume transferred during some surge events by assessing both the positive and negative glacier net volume 230 changes over specific areas. Unless specified, the extent is the surge-affected area manually drawn from the elevation change map at the surge timing calculated over the surge duration. We separate the reservoir and the receiving areas in into two distinct polygons. It is difficult to constrain precisely the initiation and termination of surges. The surge dates (Table 1) are estimated visually from two sources: the pre-processed timeseries and the interpolated elevation changes. None of these sources permits us to be sure of the exact month of start or end of the surge. We estimate the dates from interpolated elevation change (e.g. 235 Fig. 8) when computing volume transfers, such "apparent" dates are less exact but capture the overall mass transferred in our generated dataset. We may also estimate the dates from pre-processed time series (not affected by filtering and interpolation defects) for information or validation, which permits us to be more exact although we are still limited by the number of observations. For example, for the time series Fig. S2.a in the Supplement (from the Khurdopin glacier), the surge period estimate at this location from the interpolated time series would be around 2016-06 to 2019-02, against 2016-12 to around 240 late-2017 (there is no observation between 2017-06 and 2018-07, thus time series at other locations are required for a better estimate).

To compute the volume transferred, we differentiate transferred volume, we subtract the elevation at two dates. We then mask the surrounding areas. We interpolate (small) data gaps in the elevation change maps with a bilinear interpolation. Finally, the sum of elevation changes per area (reservoir or receiving area) are converted to volume via the size of pixelswe retrieve the volume by multiplying the mean elevation change with the delineated area.

The sum between of the volume changes in the two areas gives the volume imbalance. We also provide an imbalance in meter: we divide the volume imbalance by the surge-affected area. This imbalance is more representative of the corresponding uniform elevation change to provide the metric imbalance in metre (as if the imbalance was uniformly distributed on the surge-affected area). The metric imbalance is directly comparable to the elevation change uncertainty, and it permits allows us to compare the results independently of the glacier size.

3.6 Uncertainty of volume transfer estimates

We calculate indicative uncertainties of the volume transfer estimates. These uncertainties do not explicitly take into account possible errors introduced during the filtering and interpolation of each event.

255 Our uncertainty is estimated with the following formula.

$$\sigma_{\Delta V} = \sqrt{(\sigma h_{\Delta DEM}(p + 5(1 - p))A_{area})^2 + (max(d\Delta V_{-100m}, d\Delta V_{+100m}))^2}$$

The first member of the formula account for the uncertainty in average elevation difference. $\sigma h_{\Delta DEM}$ is the uncertainty in the mean elevation difference obtained by propagating the pixel-wise measurement uncertainty. The pixel-wise uncertainty is estimated from elevation differences between the interpolated ASTER DEMs and reference DEMs (SPOT5 HRS, SPOT6 and HMA DEM; details in subsection 5.1), considered as the true elevation, over four surge events (Hispar, two dates on Braldu surge, and Kunyang glaciers; Fig. 10) within the surge-affected zone. It is therefore representative of the error on glaciers, during surge events. From each dataset, we reconstruct an empirical variogram using the *SciKit GStat* Python library and all variograms are normalized by their variance and aggregated by taking the mean. We then fit the experimental variogram with a double-range Gaussian model (estimated ranges of 1.4 and 19 km) and estimate the mean elevation difference uncertainty from the number of effective samples calculated from the model with the *xDEM* Python library (Supplementary Fig. S11). A_{area} is the area of the delineated zone and p the proportion of A_{area} with valid observations (ranging from 0.92 to 1, median of 0.99). This formulation assumes that the uncertainties of spatially interpolated observations is 5 times larger than the measurement uncertainties, as in Berthier et al. (2014).

The second member of the formula estimates the volume uncertainty due to the manual delineation of the area over which the volume change is computed. $d\Delta V_{-100m}$ and $d\Delta V_{+100m}$ are the differences between the volume change estimated over the delineated area and the volume change estimated over an area with a buffer of -100 or +100 m, respectively. This assumes an uncertainty in our manual delineation of 1 pixel, which is reasonable given the strong contrast in elevation on the edges of the surge reservoir and receiving areas.

We propagate the uncertainties to the volume imbalance, assuming independent errors, with the following equation:

$$\sigma_{V,bal} = \sqrt{(\sigma_{\Delta V,reservoir})^2 + (\sigma_{\Delta V,receiving})^2}$$

The uncertainty in metric imbalance is then expressed as $\sigma_{V_surface_bal} = \frac{\sigma_{V_bal}}{A_total}$ with A_total the total area considered.

4 Results

260

265

270

275

280

4.1 Performance of the outlier filtering

We compare the filter and the temporal interpolation developed to in this study with those of Hugonnet et al. (2021) on in locations that are affected by surges, but also for all the glaciers of glaciers in the region (Fig. 6, Fig. 7). In Hugonnet et al. (2021), the iterative GP regression filtering is responsible for removing some high-amplitude surge signals (Fig. 6.c1-2, or abnormal gap A1 circled in red in Fig. 7.a). In Hugonnet et al. (2021), the kernel of the GP regression filter does not model

well the ehange in elevation change that is typically observed during surge events. The elevation change rate modelled for interpolation is much lower than surge ones, and the time length scale of the changes modelled is longer than most of the surge time-scales some of the surge events (e.g., Fig. 6.c1). Modifications of this kernel to allow for stronger changes in elevation have not proven to be efficient enough. In our workflow, the LOWESS filter behaves with varying performance, depending on the time series quality (noise, temporal density, surge amplitude). It does conserve nearly all known surge events in our study area and period, one limit case being surge events with preserves well the surge signal of 3 of the 4 events we analyse in subsection 4.3, and this observation seems to extend to a number of surge events in the Karakoram. One exception is periods of low temporal density during surge events, especially when combined to strong melt before and after the surge. A typical example of this such erroneous filtering is a part of the front of the Khurdopin glacier (FigSupplementary Fig. \$2.3.2.a). In this time series, two critical observations are filtered out around 2017, and the during the short surge. The ALPS-REML interpolation smooths the signal even further—as both LOWESS and ALPS fits are sensitive to the lack of elevation measurements at abrupt trend changes, with fewer point to constrain the fitting. Strong melt in the receiving area increases the elevation-change smoothing effect of the fits by reducing the average elevation change locally before and after the surge.

The LOWESS workflow is also sensitive to the weight estimate and noise on unfavourable terrain (in textureless and steep areasfor example), for example, resulting in more unrealistic erratic filtering than those of the original study the filtering being oversensitive to noise compared to the original workflow (red circles B1-2 in Fig. 7.b). This filter oversensitivity occurs on time series with scattered elevations, and it is often due to the correlation error score that is not very representative of the actual pixel quality: outliers may have lower uncertainties than observations close to the true elevation more accurate observations (e.g., Fig. ??.e Supplementary Fig. S2.e or S7 at 15 km). These types of locations location are not predominant in surge-affected areas, and a number of them are completely filtered out by the following stepsof the filter. The filtered-out during subsequent filtering steps. Thus, filtered areas (data gaps) and spurious elevations are more prevalent with our method, mostly over unfavourable terrain. No discontinuities caused by erroneous filtering are visible on Fig. 7.b, compared to a (red circle). We attribute this difference to the filtering with the LOWESS filter, that is more suited to preserve abrupt elevation change signal, than with the filter of Hugonnet et al. (2021) over textureless accumulation areas.

After filtering, 50% of consecutive In summary, our filter better preserves the surge signals that were filtered out in the workflow of Hugonnet et al. (2021). However, the new filter is more noise-sensitive over textureless accumulation areas and rough terrain, leading to data gaps or artifacts with large elevation changes. The preprocessing step removed 46% of the original regional dataset (number of on-glacier elevations shift from below 50 days apart to 130 days, and about 90% shift from below 9 months apart to 17 months. Said differently, nearly 40% (75pixel), and the filtering step removed a further 42% of the preprocessed dataset (69% removed in total compared to the original dataset). After filtering, nearly 30% (62%, respectively) of any date in the time series periods are between unfiltered observations less than a year (two 9 months apart (one and a half years, respectively) apart against. Before filtering, for the same percentage, it was a half-year before filtering (one year, respectively) (Fig. 2, solid orange line). The time series are about half as dense as before, temporally.

4.2 Performance of the temporal interpolation

320

325

330

340

345

The interpolation of Hugonnet et al. (2021) is a GP regression with the same kernel as for the filtering. Fig. 6.a-b1 shows edge effects at the temporal bound of the time series due to the linear member term of the kernel. The seasonal member It is noteworthy to mention that by its design, the original kernel is optimized to preserve a linear trend to extrapolate out of the observation period of each pixel. The seasonal term of the kernel creates the undulations of a one-year length scale periodicity. In comparison, our workflow shows only limited border effects. He The workflow presented in this study better fits changes in trends (ex. Fig 6.a1-2), and preserves most of the surge signal (Fig 6.c2). However, dense clusters of points are regularly over-fitted, creating wavelet artefacts at a few month scales spurious high frequency oscillations spanning typically about 6 to 12 months, as illustrated in Fig. 6.c2 around 2006 and 2011 or 6.a2 around 2006. Comparing the final interpolated elevation changes over two years (Fig. 7.c-d), our workflow can capture the complete surge signal of Hispar and Braldu glaciers (bottom-left glacier between a4 and a5, and right glacier between TSa and TSc annotated points, respectivelyred circles C1-3 in Fig. 7.c), which was not the case for the previous workflow. At these locations, the original method of Hugonnet et al. (2021) removes completely completely filters out the surge signal, filling the period with the global trend or a completely smoothed trend (e.g., Fig. ?? Supplementary Fig. S1). Moreover, several reservoir or receiving areas of the surges have weakest show smaller elevation changes with the original method, which tend to smooth remaining surge signals, both in time and in elevation (e.g., Fig. 6.c1 and FigSupplementary Fig. S2.??.d). The maximum on-glacier spatial coverage of on-glacier interpolated elevation over Karakoram is about the Karakoram is around 80% from 2005 to 2015 (Fig. 2, solid blue line). Some glaciers are more affected by data gaps than others, in agreement with areas with a low number of observations (Fig. 1).

4.3 Analysis of selected surge events

To illustrate the outputs of our method, we analyse a few four surge events that have been studied in the literature. They occur on four glaciers: Hispar, Khurdopin, Kyagar and Yazghil glaciers. Fig. 8 shows the spatio-temporal evolution of the surface elevation of selected glaciers along their centerline glaciers surface elevation along their centreline (green line on Fig. 7).d, except for Kyagar glacierout of the area)., outside the visible area of the map). Time series, extracted at regular intervals along the selected centrelines are shown in Supplement (Fig. S3 to S7).

We can observe the influence of Kunyang tributary surge that reached Hispar main glacier tongue (around kilometre 40) in early 2008 (Fig. 8.a, area a1). The surge front propagates downstream for several years with a decreasing speed propagation rate (2009-2012—Fig. 8.a, area a1), while strong thinning starts at the junction and approximatively five approximately 5 kilometres upstream of the surge front. A slight and short positive elevation change on the main trunk of Hispar up to a few hundred meters before the junction (around 49 km), starting one year after the surge reached the main trunk, may indicate mass accumulation from a blockage of the ice flow (Fig. 8.a, area a2). The time series (not presented here) confirms this thickness gain. Meanwhile, a slight and more regular build-up or thickening occurs above, upslope of 25 km (Fig. 8.a, area a6). The Hispar

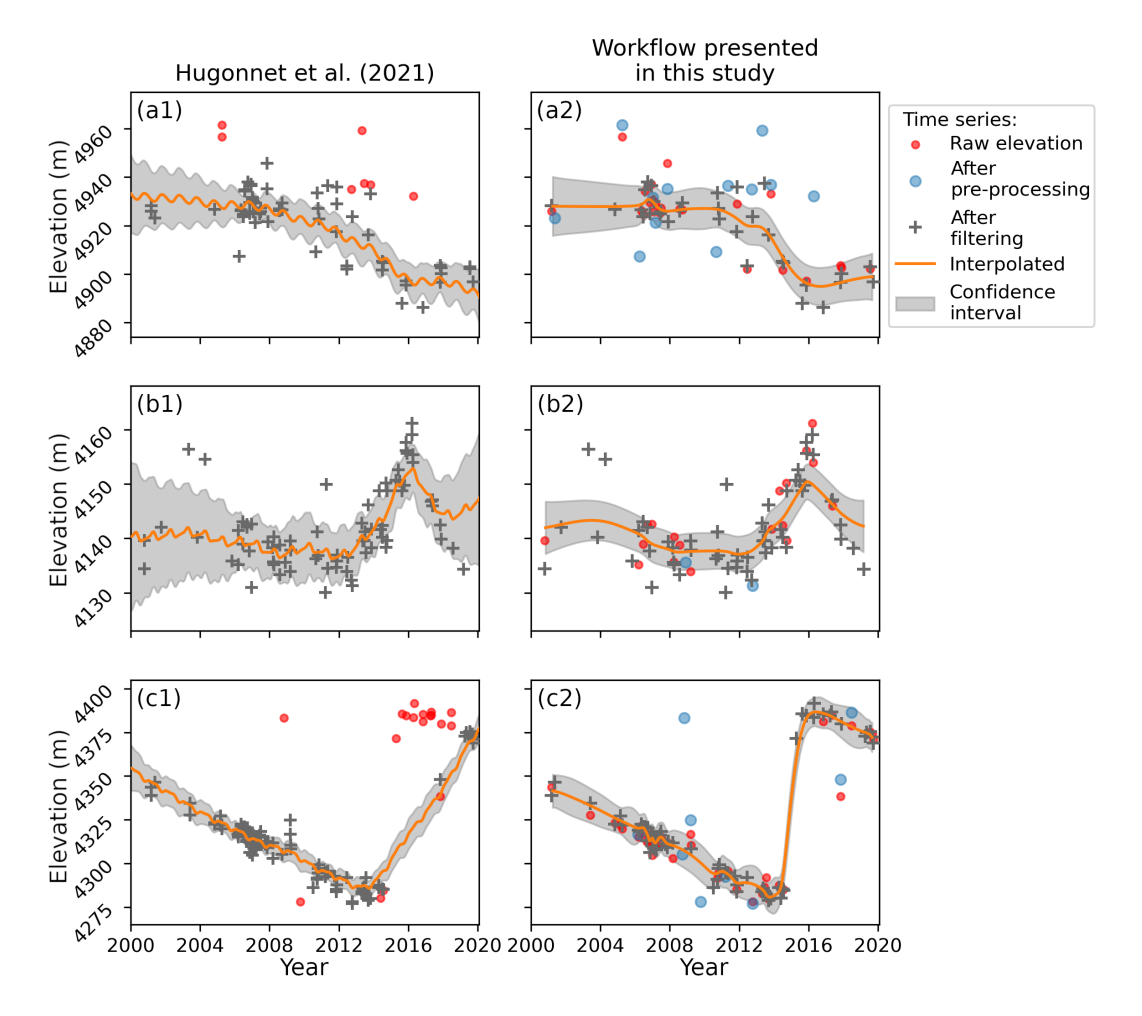


Figure 6. Comparison of pre-filter, the filter and interpolation methods of the data's processing: (a-e1a1-c1) from Hugonnet et al. (2021) against this workflow (a-e2a2-c2) the workflow presented in this study. The three time series show all show a surge around 2015, their 2015. Their location is represented on the map Fig. 7.c (points TSa-c). We avoid overlaying points for readability (i.e., points exist but are masked in lower-level time series, in legend order). The uncertainty confidence interval is valid for the interpolation only and not the whole workflow: it is the 1 σ standard deviation credible interval for GP regression (Hugonnet et al., 2021), and it is the 95% t-confidence confidence interval for ALPS-REML (this workflow). (Shekhar et al., 2021)

the lines a3 and a4 on Fig. 7.d and Fig. 8), with small mass displacement until the end of 2017, downslope of the Kunyang junction. Sharp wavelets spurious high-frequency oscillations of positive and negative elevation changes occur from mid-2013 to mid-2014, which we attribute to artefacts of our method, are visible horizontally on the Hovmöller diagram. Fig. 8.a. The time series shows dense and very scattered elevation observations at this period even on stable ground (FigSupplementary Fig. \$2.??.c), causing these artefacts. This spread may be due to tilts or undulations remaining in the DEMs. The results indicate that the dynamic balance line location is not stable in time. On the branch of the Hispar Pass (source-head of one of the main

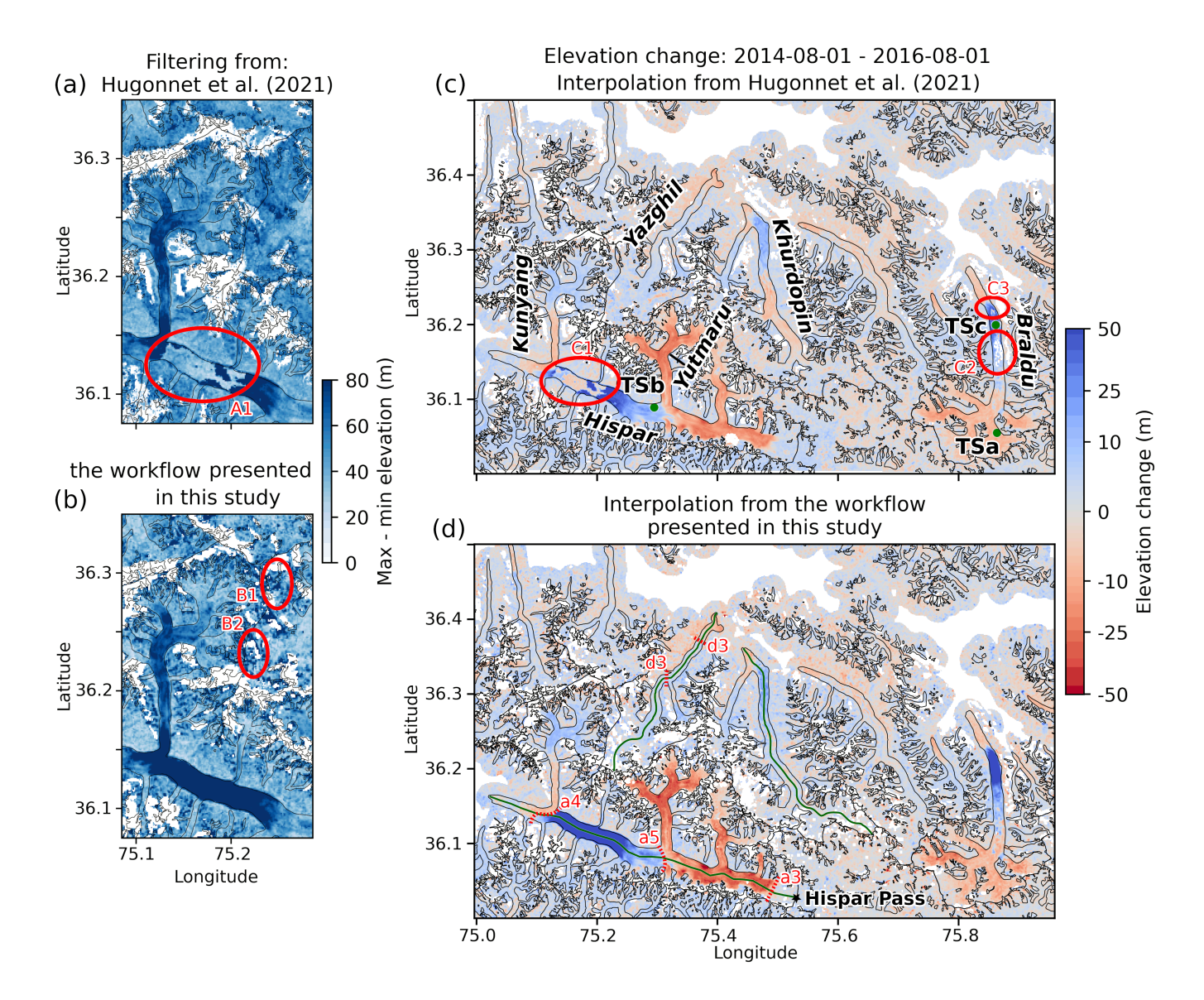


Figure 7. a-b: maps_Maps of maximum elevation change after the filter methodsfiltering. c-d: elevation_Elevation change maps over two years (Hispar glacier surge period). The green points and their labels (TSa-c) in c) correspond to the localisation of the time series in Fig. 6 (a-c). Their coordinates are (EPSG:4326): TSa (75.863, 36.055), TSb (75.295,36.089) and TSc (75.861,36.200). The green lines on d are the eenterlines centrelines of the Hispar glacier studied glaciers. The red circles (bottom left, branch of the Hispar PassA1-C3), Yazghil glacier (center left) and Khurdopin glacier the dotted lines (center a 2.5 and d3) show or delimitate areas discussed in the text.

branches, location on Fig. 7.d), the reservoir area extends from 5 km of from the pass, at an icefall (line a3 on Fig. 7.d and Fig. 8), down to 20 km from the pass at the junction with the Yutmaru tributary in the first part of the surge. From the end of 2015 to the end termination of the surge, it then extends the reservoir area limit propagates down by 5-10 more kilometres down

kilometres (below the junction) (line a5 on Fig. 7.d and Fig. 8). We plot an elevation time series at this location (Fig. 6.b2, location TSb on Fig. 7.c)). The higher limit of the reservoir area stops at an icefall. The . The receiving area extends from the same location at 20 km at first and 25 km thenend of the reservoir area at 20-25 km from the pass along the centreline, down to nearly 40 km from the pass at the junction with the Kunyang tributary (line a4 on Fig. 7.d and Fig. 8.a).

We now assess the volume of ice transferred during the surge, from 2014-01-01 to 2016-09-01. We calculate a volume change over the reservoir area of $-2411-2421 \pm 374 \times 10^6$ m³, and of $3110-3108 \pm 177 \times 10^6$ m³ over the receiving area (Table 1). The imbalance resulting is of 700 resulting imbalance is $687 \pm 414 \times 10^6$ m³, which represents an evenly distributed layer of $4.55 \pm 4.46 \pm 2.69$ m thick over the whole surge-affected area. The difference between volume gain and loss, or imbalance, is unexpected as the surge occurs over a short time period and mass should be conserved in a first approximation. The imbalance is quite similar when using two filtered ASTER DEMs over a similar period over this surge, instead of interpolated.

We analyse more briefly the other surge events visible on Fig. 8. Khurdopin glacier has a gradual surge onsetor pre-surge phase, visible like a gradual positive elevation change slowly expending downward strong mid-glacier thickening signal until the surge onset. The distinct area of positive elevation-change trend extends down-glacier during at least 15 years (Fig. 8.b., area b1). The "This mass build-up front" extends from about 27 may be the geometry readjustment of the glacier in its quiescent phase, after the previous surge in 1998 (Quincey et al., 2011). The lower limit of this build-up area propagates downward from about 25.5 km of the glacier source in 2002 to about 33 km in 2015, representing a regular advance of about 460 head in 2001 to about 33.5 km in 2015. The limit advances approximately 600 m per year during this period, which is approximately 6 about 7 times faster than the surface velocity (measured 2 km upstream of the front), according to velocities (temporal baseline from 300 to 430 days) from the NASA MEaSURES ITS_LIVE project repository (Gardner et al., 2022). During this period, we do not observe a clear mass transfer from an upper reservoir area, which thus seems different from a slow surge onset. The upper limit of the build-up area and then of (which will mostly become the reservoir area) is stable in time, at the bottom of an icefall. The actual-two icefalls for the two main branches just above their junction.

The surge starts in 2016, the surge front continuing the "pre-surge" front with the build-up front becoming a surge front with a higher propagation rate. Both our filter and interpolation methods here fail to eapture fully fully capture the surge signal of the receiving area (see discussion section 5.2). It This failure leads to an apparent surge end in early-2019 on interpolated data, which is overestimated by about a year and a half according to non-interpolated time series (FigSupplementary Fig. S2.??.a). A distinct and local positive elevation change pattern in is visible after the surge around kilometre 23 (Fig. 8.b, area b2).

Kyagar glacier is located about 110 km to the East east of the other glaciers (Fig. 1). A slight mass buildup build-up is visible since the beginning of the time series in the first ten-10 kilometres of the glacier, and extends up down to about 14 km a few years before the surge. It starts around the end of (Fig. 8.c, area c1). The surge as visible on interpolated data starts in 2013 or the start beginning of 2014, and ends in late 2015, around 2016 (Fig. 8.c, area c2). However, the actual surge is certainly shorter. The beginning of the surge appears sooner in the interpolated time series, and the end is also represented nearly a year later from what is visible on the non-interpolated time series of most of the receiving area. During the surge period, there are about

1-2 observations per year. There is an area where An area or poor quality in the ASTER time series is of bad quality resulting in some results in artefacts after processing, at 5 km from the glacier sourcehead, which is located around the equilibrium line of the glacier. The reservoir area seems to extends upward of this area. This issue biases (Fig. 8.c, area c3). This area seems to be in the reservoir area, therefore causing a bias in the volume transfer calculation. We manually draw a mask to remove artefacts for a better estimate (Table 1).

395

Our dataset captures a full surge cycle of Yazghil glacier. On this glacier, the surge signal has a low amplitude (approximately ten metres) compared to the time series, and thus noise is often overfitted. This results resulting in frequent interpolation artefacts. Some seasonal signal seems also to be fitted, for example during the period 2013-2016 thanks to denser and consistent time series (horizontal lines on the Hovmöller diagramFig. 8.d). A surge starts in late-around August to November 2003 and ends in late around October 2006 or early to February 2007 (Fig. 8.d, area d1), and a new surge starts in 2017 or early 2018-2016 or 2017 (the end is not captured; 8.d area d2). One of the tributaries of Yazghil glacier (junction at km 18) is also surge type, and seems to have surged during our study period in about 2008-2013. The buildup and emptying of the first surge seems weaker than the second one, and extends less up-glacier of the junction, compared to the second surge The build-up phase of the second surge is visible, representing about half of the quiescence phase (Fig. 8.d area d3, delimited by dotted lines d3 on Fig. 7.d). This may be related to the effect of the tributaries of Yazghil glacier (junction at km 18) is also surge-type, and seems to have surged during our study period in about 2008-2013.

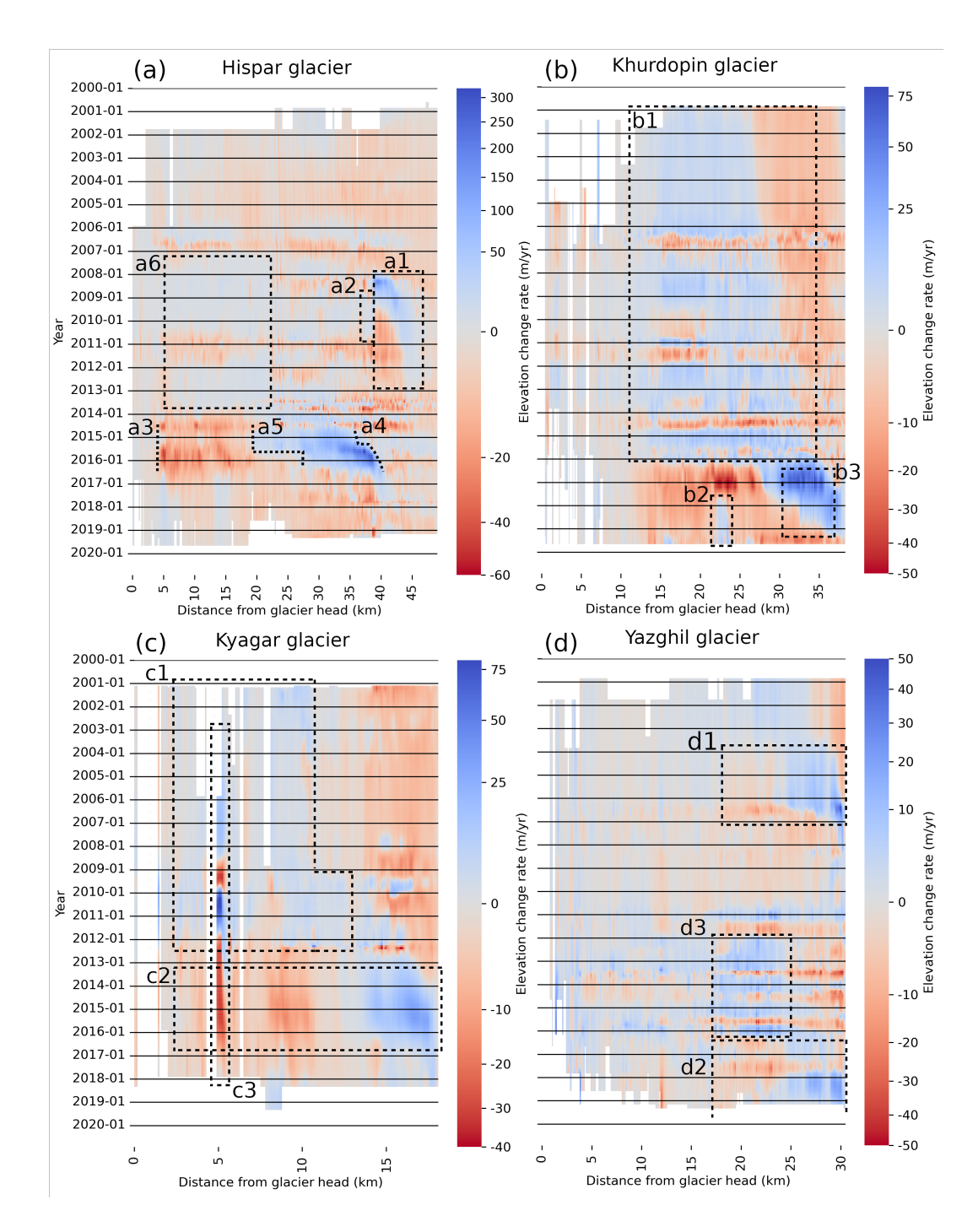


Figure 8. Hovmöller diagrams, spatio-temporal evolution of the interpolated a-d: Interpolated surface elevation time series along the centreline of four glaciers. The elevation change is sampled on the centerline of the glacier (in green in Fig. 7.d). Glaciers flow from left to right on the different panels. Note that the colorscales represent different elevation change rate amplitude and that they are non linear.

Glacier	Date start	Date end	Reservoir	Receiving	
RGI 7.0 code			vol. change	vol. change	
KGI 7.0 code	[time series]	[time series]	[Surface area]	[Surface area]	
Hispar	2014-01	2016-09	$\frac{-2411 \times 10^6 \text{ m}^3}{2}$ $-2421 \pm 374 \times 10^6 \text{ m}^3$	$\frac{3110 \times 10^6 \text{ m}^3}{3108 \pm 177 \times 10^6 \text{ m}^3}$	687
21670	[2014-05]	[2016-06]	$[106 \text{ km}^2]$	[48 km ²]	4
Yazghil	2003-07	2007-01	$-32 \times 10^6 \text{ m}^3$ $-32 \pm 30 \times 10^6 \text{ m}^3$	$63 \times 10^6 \text{ m}^3$ $63 \pm 26 \times 10^6 \text{ m}^3$	32
21865	[2004-01]	[2006-08]	[8 km ²]	$[6 \text{ km}^2]$	2
Khurdopin	2016-03	2019-03	$\frac{-801 \times 10^6 \text{ m}^3}{-801 \times 10^6 \text{ m}^3}$ $-813 \pm 136 \times 10^6 \text{ m}^3$	$\frac{711 \times 10^6 \text{ m}^3}{710 \times 10^6 \text{ m}^3}$ $713 \pm 64 \times 10^6 \text{ m}^3$	-100
14958	[2016-04]	[2017-07]	[33 km ²]	$[15 \text{ km}^2]$	-
Kyagar	2012-11	2017-01	$\frac{-271 \times 10^6 \text{ m}^3}{2}$ $-271 \pm 92 \times 10^6 \text{ m}^3$	$\frac{267 \times 10^6 \text{ m}^3}{2} 269 \pm 55 \times 10^6 \text{ m}^3$	-2 =
14958	[2013-10]	[2015-12]	$[21 \text{ km}^2]$	$[8 \text{ km}^2]$	-0
Kyagar without			$\frac{-228 \times 10^6 \text{ m}^3}{2}$ $-217 \pm 116 \times 10^6 \text{ m}^3$	$\frac{267 \times 10^6 \text{ m}^3}{267 \times 10^6 \text{ m}^3} = 269 \pm 55 \times 10^6 \text{ m}^3$	52 =
artefact		_	$[20 \text{ km}^2]$	[8 km ²]	1

Table 1. Timing and volume transferred volume of the surges for of four glaciers in the study area. The main dates are given according to the Hovmöller diagrams on interpolated changes elevation time series on the centrelines (Figure 8). We compute the volume transferred volume ("vol. change") from interpolated DEMs at these dates to capture estimate the corresponding volume change from both reservoir and receiving areas. The dates between brackets are those estimated visually on non-interpolated time series, thus less smoothed, given for indication. They are not accurate to the month due to ASTER acquisition dates. Volume changes are in x10⁶ m³. The volume change and the imbalance computation method is detailed in the subsection 3.5. The data gap is given in percentage of For these glaciers, the surge-affected area. The percentage between brackets is the of data gap proportion remaining after a the workflow presented in this study is ranging from 0 to 5.6% (median of 1.4%), and after bilinear interpolation it is of the elevation change 0 to 0.8% (median of 0.2%). The prefix of RGI codes is "RGI2000-v7.0-G-14-".

5 Discussion

5.1 Processing quality

The uncertainty estimate of the ALPS-REML algorithm cannot represent the ability of the filter to keep true elevations and remove outliers. To assess the quality of our results, we 1) compare our interpolated elevations with external DEMs produced from high resolution satellite imagery, and 2) test the sensitivity of the interpolation to data gaps. Note that the uncertainty estimate of the ALPS-REML algorithm, which is represented in the figures, does not represent the uncertainty of the whole workflow.

First, we compare the interpolated elevation with external DEMs, produced from optical very-high resolution satellite imagery (Fig. 9). This comparison provides a validation of estimated elevation during a few surge events. We use SPOT5 HRS and SPOT6 DEMs generated by Berthier and Brun (2019), and along-track HMA DEMs (Shean, 2017) (list in Table S2 of the Supplement). We co-register each external DEM on the ASTER interpolation . The NMAD score on stable terrain. The Normalized Median Absolute Deviation (NMAD) after co-registration ranges from 6.8 to 15.6 m (median 7.4 m), which shows a good agreement with discrepancies of a few meters. Extreme cases occur locally with differences reaching tens of meters, but it is generally unclear which dataset is flawed. The case study of Khurdopin glacier surge , discussed above, shows however that a discrepancy shows that a wrong estimate of a hundred meters of our workflow is credible on exceptional events . and at precise dates during the surge (Supplementary Fig. S2.a). The map of elevation differences shows moderate differences overall, which ean may be important locally (Fig. 10). Systematic differences appear over the whole glaciers glacier; e.g., the median difference is of -4.3 m (standard deviation of 9.7 m) on Hispar glacier on 2015-10-13, -5.2 m (standard deviation of 8.7) on Braldu glacier on 2015-11-28. Larger local differences are located around the surge front: e.g., up to 24 m at Hispar surge front on 2015-10-13. We compute the percentile of elevation change The elevation difference values during a surge event and during quiescence (Table ??). The results do not show important difference differences at the scale of the surge-affected area . (Fig. 11). The discrepancy associated to with a surge period is overall of the same magnitude as other noise, considering the large standard deviations dispersions.

Percentile: 2nd 10th 50th (median) 90th 90th During surge -17.3 m (SD 12.0 m) -7.5 m (SD 5.9 m) -0.1 m (SD 3.6 m) 13.8 m (SD 13.6 m) 28.7 m (SD 29.6 m) Quiescence -16.2 m (SD 9.3 m) -8.5 m (SD 5.1 m) -2.1 m (SD 3.8 m) 3.5 m (SD 3.2 m) 11.4 m (SD 6.1 m) Average percentiles of elevation difference between reference DEMs and interpolated ASTER DEMs. We compute independently the percentile over each surge-affected area of Hispar glacier, of Kunyang glacier (Hispar glacier tributary) and of Braldu glacier. We then get the average of the percentiles according to the surge phases of the glaciers. *SD* are standard deviations. There are four reference DEM per surge phase: SPOT5, SPOT6 and 2x HMA DEM during surges; 3x SPOT 5 and SPOT6 in quiescence phase.

One of the main limitations of our results is the relatively sparse observations in the time domain. Herecomes from the relative temporal sparsity of the input observations. Here, we investigate the impact of data gaps on our interpolated time series. The spatial data gap on-glacier at the regional scale is nearly 20% at best over Some parts of our study area, during 11 years (from 2005 to 2016). It rises to 40% of data gap to capture five more years (Fig. 2). A number of surge events are interpolated from temporally low-density time series are characterised by a low temporal density of observations during surge events (e.g., less than 3 observations per year) or thus with large data gaps, mostly clustered over specific Karakoram parts (Fig. 1). In such situations, our method of filtering and interpolation usually leads to an underestimate of the volume transferred transferred volume and an overestimate of the surge duration (e.g., twice its duration for the Kyagar glacier), even when relying on the filtered time series and not on the interpolated one. Onset and end dates cannot be precise to a few months for a surging area with only one or two observations per year (e.g., the case study of the Kyagar glacier surge).

450

455

To test the sensitivity of the ALPS-REML method to data gapgaps, we interpolate an elevation time series after removing all points in a 450-day moving window (Fig. 12). Each iteration results in a period of at least 450 days without observation. For the selected time series a) and c), the test shows strong smoothing, although the surge signal is still visible over large time frames. The interpolated dates of the surge onset (ending, respectively respectively ending) are advanced (delayed, respectively respectively delayed) up to two years compared to the original interpolation. The surge elevation change can be underestimated

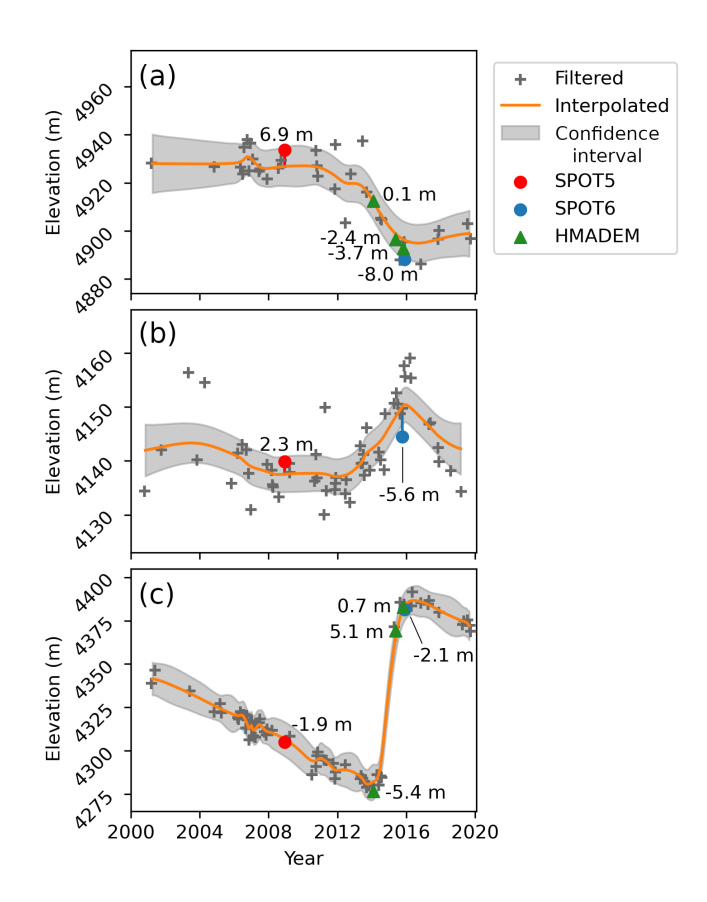


Figure 9. a-c: Comparison of elevation between elevations from SPOT DEMs (SPOT5 HRS and SPOT6) and HMA DEMs against and ASTER elevations interpolated at the same dates. The time series are identical to previous ones (TSa-c in the panel order, Fig. 7.c).

up to about by up to 20 meters. This can be larger for larger time gaps or surges with stronger elevation changes before or after the surge. Case b) is specific, as it lies close to the dynamic balance line (in the receiving area at an early stage of the surge, and then in the reservoir area). The surge signal is completely smoothed out when the data gaps occur in the middle of the surge. Other specific cases of surgessurge cases, with limited elevation changes but with strong melt or strong build-ups before or after the surge, could be prone to the same problem. An ASTER dataset generated with smaller noises and errors could improve the interpolated dataset ability to capture surges.

5.2 Comparison of surge characteristics with the literature

460

We compare our analysis of the selected surge events with the literature.

The advance of Kunyang tributary during its surge on Hispar main trunk was already well documented, and our observations align well with the previous ones (Paul et al., 2017). Regarding the surge of the main trunk of Hispar described in section 4.3, our date estimates (mid-2014 from both interpolated and pre-processed time series (early-2014 to mid-2016) are very close to

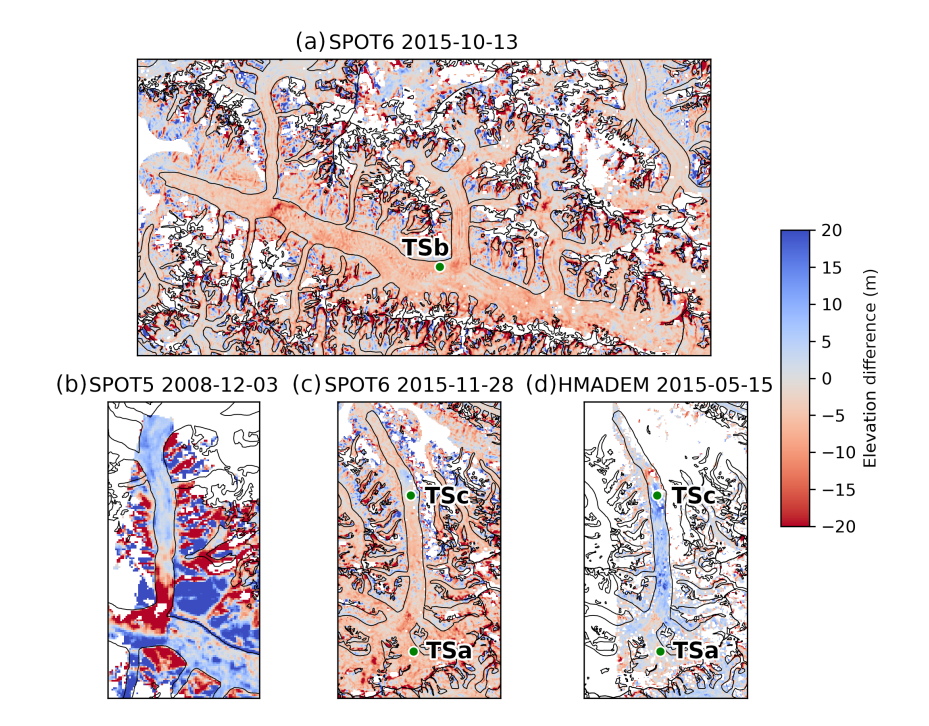


Figure 10. Difference of elevation a-d: Elevation difference between SPOT DEMs (SPOT5 HRS and SPOT6) and HMA DEMs against ASTER elevations. DEMs interpolated at the same dates. The areas selected are the Hispar glacier (a. surge in 2014-2016), its Kunyang tributary (b. surge in 2007-2008), and two over the Braldu glacier (c-d, surge in 2013-2016). The panels have the same colour range. The green dots show sampled time series (Fig. 6, 7.c and 9).

the previous study date date estimated in previous studies (autumn 2014 to mid-2016), which were based on remotely sensed velocities (Paul et al., 2017; Guo et al., 2020) (Guo et al., 2020; Paul et al., 2017). Paul et al. (2017) notices a 6-month stop of the surge front around 35 km, up to mid-2015. It: it is slightly visible here at a similar time (Fig. 8 a, line a4). The fact that the reservoir area does not extends extend above the icefall has already been observed on other glaciers, including Khurdopin in our study (Nolan et al., 2021; Echelmeyer et al., 1987). This can be due to the lower drawdown that the kinematic disconnection the icefall creates Nolan et al. (2021); Terleth et al. (2021). The displacement of the dynamic balance line of during this surge has not been mentioned in other studies , as it is certainly only visible with elevation change data and at short timescale. for Hispar, as the data they use (velocities and a limited number of DEMs spaced in time) may not permit to observe this phenomena (Guo et al., 2020; Paul et al., 2017; Rashid et al., 2018). However, the phenomenon has already been reported and attributed to variations in driving stress (Burgess et al., 2012). Bhambri et al. (2022) estimate volume changes over the period 2014-2020 from ASTER DEMs of -2785 x106 m³ in the reservoir area, and 2581.6 \pm 465 x106 m³ in the receiving area. Our estimates over the surge dates are similar estimate for the reservoir area volume change, -2411 x106 m³ (about differ by 13% difference; Table 1). We find a larger difference, and 20% in the receiving area, with 3110 x106 m³ (20%), for which post-surge melt (Table 1). The smaller volume estimated by Bhambri et al. (2022) may be explained by the melting of the deposited ice volume likely

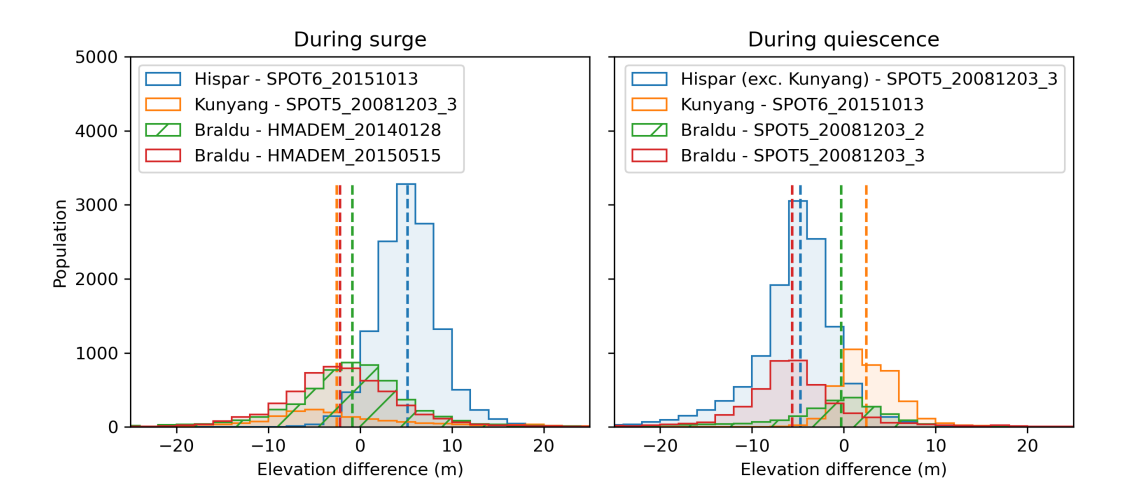


Figure 11. Test Histograms of interpolation robustness. For the three selected time series elevation difference between the reference DEMs and the DEMs of Figour workflow interpolated at the same dates. 6, we remove points during 450 continuous days over a moving window for which We consider only surge-affected areas. Vertical dotted lines are the median of each interpolation histogram. The largest median is in orange 5.18 m (resp. -5.63 m) during surge (resp. during quiescence).

explain partially the smaller volume of Bhambri et al. (2022). Accordingly, over a longer period up to during the three or four years that separate the surge termination and elevation observations. If we extend the period of volume change calculation from 2014-10 to 2018-08 (the latest date before large data gaps at the end of the time series, from 2014-01 to 2018-08, the volume change estimate is closer to their result: -2736 in our time series) to better match that of Bhambri et al. (2022), we estimate a volume change of -2255 ± 181 / $2793 - 2634 \pm 410 \times 10^6$ m³ (2% and 819% and 2% difference, respectively). The closer to their estimate. The differences are within uncertainties, although there is a two years difference between the two estimates periods.

485

490

The difference between our estimated volume gain and loss is equivalent to a layer of 4.46 ± 2.69 m thickness over the surge area. This imbalance is unexpected as the surge occurs over a short time period and mass should be roughly conserved. The imbalance is quite similar when using two filtered ASTER DEMs over a similar period, instead of the interpolated series, or when calculated over the full glacier system instead of over the delineated reservoir/receiving areas. The impact of crevasse opening during the surge on the apparent surface elevation have has not been assessed.

The gradual surge onset we observe for Khurdopin glaciercorresponds to the observations of several studies (Steiner et al., 2018; Imran at 495—, especially regarding our imbalance, but it may represent a non-negligible volume. The propagation of the pre-surge or thickening front have however opening of crevasses can be equivalent to up to 0.2 m thickness over regional scale of the Greenland Ice Sheet (Chudley et al., 2025). As inland parts of these regions are largely crevasse-free, we can expect such volume to be significantly larger over the highly crevassed post-surge surface of Hispar glacier, at least one meter magnitude. By mid-2018 our imbalance is close to zero, as well as is the imbalance of Bhambri et al. (2022) with an end term in 2020,

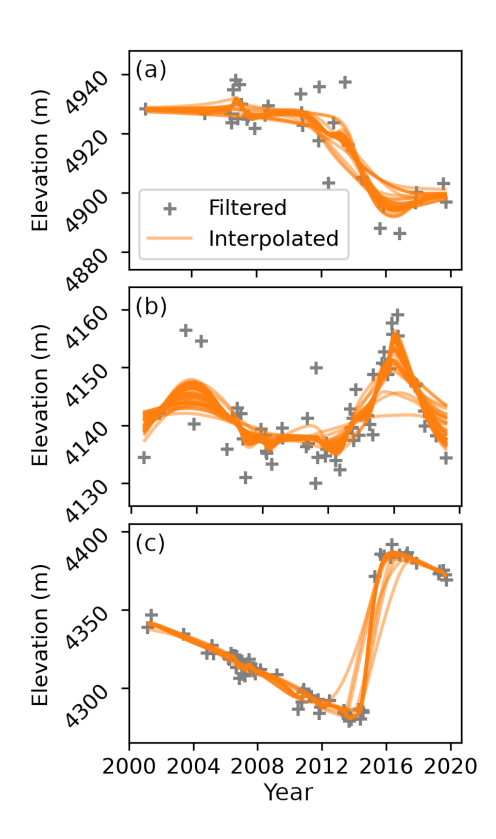


Figure 12. Sensitivity of our interpolation method to large data gaps. For the three selected time series (TSa-c of Fig. 6 and location visible on Fig. 7.c), we remove points during 450 continuous days over a moving window and run the interpolation, displayed with orange lines.

when a number of crevasses have already closed. Khurdopin and Kyagar glaciers were already highly crevassed before the surge, and such crevasse opening effect may be less important.

505

510

We now discuss the recent surge of Khurdopin glacier. The geometry readjustment and the propagation of a build-up front during quiescence has not been observed. The surge on this glacier, to our knowledge. The existence of kinematic waves or surge fronts that propagate the surge instability have regularly been observed on other surges (e.g., Cuffey and Paterson, 2010; Kotlyakov et , with unclear definition of the phenomena. For Khurdopin glacier, the mechanism seems different from both a kinematic wave or a slow surge onset. As opposed to these processes, here we observe a constant thickening after the downward extension of the build-up area with no upper reservoir area drained. Turrin et al. (2013) observed, with velocity data, the propagation of a surge front (moving as a kinematic wave) several years before the surge of Bering glacier, triggered by the passing of the front through the reservoir area. The build-up lower limit for Khurdopin also propagated faster than the surface velocity. The surge started in October 2016 according to Imran and Ahmad (2021), a bit about 7 months later than our spring 2016 estimate (Table 1), and late August 2015 according to Steiner et al. (2018). Steiner et al. (2018) estimate the volume received in the receiving area at 1182 x10⁶ m³ during late August 2015 (elevation extrapolated linearly from TanDEM-X in 2011) to May 2017

(ASTER) data, after reassessment of the estimate (Jakob Steiner, personal communication). Our estimate over a similar period (2015-09-01 to 2017-06-01 is 425) is $426 \pm 34 \times 10^6 \text{ m}^3$. However, both our Both estimates do not agree, although we do not have an uncertainty estimate for one volume. Our filter and interpolation methods here fail to capture fully fail to fully capture the surge signal of the receiving area, in the lower part of the glacier (Fig. 8.b area b3). This failure is due to a low point density combined with a strong thinning signal after the surge (Fig. ??.aSupplementary Fig. S2.a, in 2017). The filter workflow did remove-filtering workflow removes some of the 2-3 DEM acquisitions over 2017 and 2018 with, which have credible values. May 2017 is one of the most unfavourable period with up to about 100 m of the month with the largest difference between the DEM observations and the interpolation, with an elevation change underestimation compared with the pre-filtered data. Over such areas that reaches 100 m compared to the pre-processed time series. Over a portion of the receiving area, the apparent surge signal duration after interpolation is about 3 years instead of less than approximately 1 year on pre-processed time series, and may miss locally a maximum of 40 m (about 30%) of the total elevation change surge elevation amplitude over these three years. Our estimate of the volume transferred -801 / 711 x 10⁶ m³, is thus slightly transferred volume in Table 1 is thus underestimated in the receiving area. Our uncertainty estimate is also largely underestimated, as it does not take into account the erroneous filtering. The difference of pre-filtered the pre-processed DEMs from 2015-08-20 to and 2017-05-21 shows a cumulative positive mass change of 648 volume change of 650 x 10⁶ m³. It is 152 153% more than with the interpolation, still-yet nearly half of the estimate of Steiner et al. (2018) which may be also partially overestimated due to their linear extrapolationas the gradual surge onset extends further down-glacier from the, as the 2000-2011 trend does not accounts for the later build-up front propagation that we observe. The maximum thickness gain noted by Steiner et al. (2018) was 160 m over this period, against 122 m with our pre-filtered pre-processed DEMs (70 m on interpolated DEMs). This shows the limit of our method in The case of Khurdopin surge shows that our workflow may be inefficient to preserve a surge signal, in the case of a low number of DEMs during surge events and strong thinning signals out of observations, aggravated by strong thinning outside the surge period.

515

520

525

530

535

540

545

Kyagar glacier is located in an area of poor ASTER coverage, compared to other selected glaciers (Fig. 1). During the surge period, there are about 1-2 observations per year, which leads the interpolation to smooth to a smoothing of the surge signal during interpolation. Thus, the onset and ending are visible around end-2012 and early-2017 on interpolated data, while non-interpolated time series leads to the more restricted pre-processed time series lead to a more restricted estimate of mid or end-2013 to end-2015 estimates. (sooner observation in October after a 14-month data gap) to December 2015. Round et al. (2017) uses satellite imagery to compute velocities and describe precisely precisely describe the surge development. They find a surge onset in May 2014 after a pre-surge acceleration of 2.5 years, and a surge end between July and August 2015 with limited deceleration later. Li et al. (2023) find very similar timings, plus a continuing deceleration in 2016-2019. Gao et al. (2024) report similar timing, although considering a re-acceleration in 2016 as part of the surge. Gao et al. (2024) estimated the volume transported from ASTER DEMs. Over During July 2012 to December 2017, they estimate the received volume at to be $321 \pm 12 \times 10^6 \text{ m}^3$, against 260 compared to $262 \pm 46 \times 10^6 \text{ m}^3$ with our interpolated data. Their reservoir area volume change estimate is $-383 \pm 30 \times 10^6 \text{ m}^3$, against $-328-326 \pm 96 \times 10^6 \text{ m}^3$ for our dataset over the same dates and approximative area

($-285-283\pm104 \text{ x}10^6 \text{ m}^3$ with bilinear interpolation of the artefact area affected by artefacts). It represents differences in volume transferred estimate of 19% and 14%. The study states a glacier mass balance of $0.26\pm0.02 \text{ m}$ w.e. a^{-1} over the same period. After hypsometric interpolation, we find -0.26 m w.e. a^{-1} , 0.01 m w.e. a^{-1} after manual removal of artefacts: transferred volume estimate of 18% and 15%.

Yazghil glacier has not been studied a lot. Velocities from Bhambri et al. (2017) show a velocity increase during the first surge we capture, and lower velocities the following years. They date the surge in 2006. The study estimate extensively studied.

Bhambri et al. (2017) date the last surge in 2006, with a gradual increase in velocities before this year. The study estimates from 1972-2016 data that the Yazghil glacier has a cycle length (surge repetition period, including quiescence and surge durations) of about 8 years, one of among the shortest surge cycles in HMA (Bhambri et al., 2017; Sun et al., 2022; Vale et al., 2021; Yao et al., 2023). The next surge, which was expected to occur around 2014 based on the cycle length, had not started by the end of 2016, according to the study. Our data suggest that it started 1-2 years later, implying a longer quiescence phase of 11-13 years. In addition to the case of Hispar and Kunyang glaciers described above, some blocking effects suspected here have already been observed in this region (Paul, 2015) for this cycle.

Overall, the dataset produced by our workflow compares well with the existing observations from the literature. The surge dates and the estimated volume transferred are in agreement transferred volume agree, except for the dating of the date of Kyagar surge and the transferred volume estimate of the of Khurdopin surge (Table 1). The order of magnitude of the imbalances corresponds to the order of magnitude of the measurement uncertainty. For the two critical cases (Kyagar and Khurdopin surges), the limit of the workflow occurs in workflow shows its limitations in the case of a low number of DEMs, worsened in the case of a strong thinning signal out of outside the surge period (Khurdopin surge). Our dataset offers new insights on some undescribed processes in these studies, such as the displacement of the dynamic balance line of the Hispar surge or the propagation of a pre-surge bulge front of the surge front during the build-up phase preceding Khurdopin surge.

5.3 Elevation change comparison

550

555

560

580

We assess the difference differences in elevation change estimate between the processing workflow from of Hugonnet et al. (2021) and this workflow. Previous figures showed local differences, here we compare the elevation changes of pixels belonging to eight surge events (Fig. 13, individual graphs in appendix Fig. ??). We observe on Supplementary Fig. S9). The figure highlights the strong smoothing of the original dataseteutting out surge signals in receiving areas (with, which tends to filter the positive elevation changes), that occurring in surge receiving areas, which are better interpolated by our workflow (Fig. 13 zone A). There is no symmetric pattern No symmetric pattern is visible for negative changes in reservoir areas, probably because of due to the smaller rates of elevation changes. It is mostly representative of This erroneous filtering is mostly occurring for surges with important and rapid elevation changes: surges of the Hispar, Braldu, and Kunyang glaciers (Fig. ??Supplementary Fig. S9), and to a lesser extent of the Khurdopin glacier surge. For such glaciers, major differences in total volume change are expected. This is clear in the volumes transferred transferred volume estimates from the original dataset of Hugonnet et al.

(2021) on Hispar and Khurdopin glacier surges (Fig. ??Supplementary Table S1). Other glaciers also have smaller estimated volumes than with our method, but with smaller discrepancies. Compared with Hugonnet et al. (2021), our method finds larger absolute rates of elevations elevation changes (pattern B on Figure 13), probably due to the stronger smoothing of Hugonnet et al. (2021) (e.g., Fig. 6.a1 or FigSupplementary Fig. S2.??.d). Our On the other hand, our method creates some artefacts, especially in the accumulation area areas where elevation changes are close to zero (zone C on figure 13). This is the case for Kyagar and Braldu glacier surges (Fig. ??Supplementary Fig. S9).

This figure also illustrates non-uniform elevation change patterns common to all the surges here the unequal distribution of elevation changes between the reservoir and receiving areas, which is observed for all analyzed surges (Fig. 13). The elevation changes are Elevation changes are consistently much larger in the receiving area whether the glacier front is advancing or not. This is balanced by the extent of the reservoir areas which are larger than those of the receiving area areas.

At-On a larger scale, we compare the individual glacier average elevation change between Hugonnet et al. (2021) and this workflow for the period 2005-2015 (Figure ??Supplementary Figure S10). The mean elevation changes are more negative with our workflow (by about 0.44 m for the median value). The discrepancy is larger for surge-type glaciers than for non-surge-type ones compared to non surge-type glaciers (0.57 and 0.31 m with standard deviations of 1.1 and 1.02 m, respectively). Considering the better retrieval of positive elevation changes of our workflow for surges, we would expect a positive discrepancy for surge-type glaciers. A number of glaciers have artefacts in our dataset, especially negative elevation changes in accumulation areas. At large scale and regional scale and possibly glacier scale, the noise impact may exceeds impact of noise may exceed the impact of the better retrieval improved estimate in areas of positive changes of the few, due to the small number of surge events happening during this period. For calculating geodetic glacier mass balance, the Hugonnet et al. (2021) dataset is therefore the preferred choice for non-surge-type glaciers or quiescent periods, and a validation of the elevation interpolated by our method is recommended.

5.4 Methodological Insights and Modifications Applicability for other datasets

585

590

595

600

605

610

615

In the development of the workflow, we first tried adapting Gaussian Process Regression (GP regression) like the original study instead of ALPS. Our limitation with GP regression lies in the kernel definition which is done according to the variance of elevation changes. Each surge event is different in variances, which is also very different from the data variance in quiescent periods or on non-surge-type glaciers. We tried different settings of the kernels, that differs from the study of Hugonnet et al. (2021). We removed the seasonal component of the model (exponential sine-squared (ESS) kernel). The length scale and the magnitude parameters of the remaining components were manually tuned after testing. We added radial basis function (RBF) components of length scales of few months and with a variance of a few tens/hundreds of square meters. The kernels that provided a suitable interpolation were slightly outperformed by the ALPS-REML algorithm. This could be reevaluated for other datasets (for e.g. less noisy), more complex GP regression processes or future advances.

Finally, we We discuss here the feasibility to modify of modifying the proposed workflow to be used on with different datasets, possibly including several data sources to increase temporal resolution (i.e., from DEMs from different sensors).

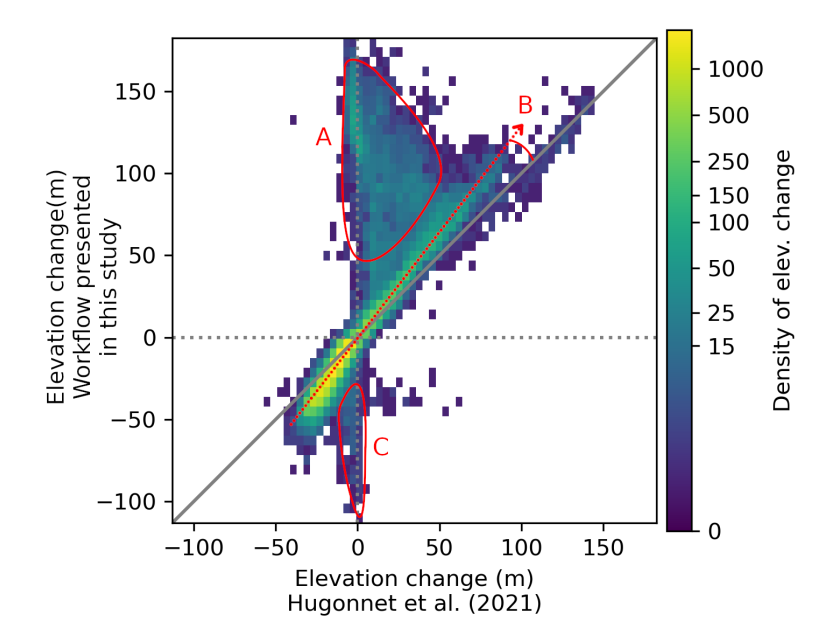


Figure 13. Histogram of interpolated elevation change comparison over 8 surges between the original processing from Hugonnet et al. (2021) and this workflow. The superimposed histograms of the 8 surge events are represented individually in appendix-Fig. ??S9 of the Supplement. The elevation changes are retrieved over the surge-affected areas and the surge period estimated from the Hovmöller diagrams interpolated elevation time series on the centrelines. The areas and trends designated in red are discussed in subsection 5.3. They highlight areas of this large surge smoothing or removal (zone A) or overall smoothing of elevation changes (trend B) by the original method (Hugonnet et al., 2021), and artefacts created by the presented workflow (zone C).

Even in the case of a similar ASTER DEM dataset processed differently, with lower noise/higher precision, several changes may be done made to adapt the filtering. A diminution of the span parameter along with a a-diminution of the filter threshold in the LOWESS workflow should be tested. Abandoning morphological erosion should also be considered, as it answers to the behaviour of our specific photogrammetric processing. It may not be beneficial for DEMs where outliers does less alter neighbouring pixels, regarding the. It addresses an issue specific to the photogrammetric processing which tend to affect pixels neighbouring outliers. Deleting this step would be beneficial given the large number of pixels it removes. The use of weighting could also be abandoned in the case of more precise DEMs, as the uncertainty values are not completely representative of the confidence in the measurement. The ALPS-REML prediction parameters could remain as it is, although other values of unchanged, although the hyperparameters degree of the basis functions p and the order of penalty q can be modified to adjust the smoothing and border effects. More complex considerations would be required in the case of several data sources. More particularly, the weighting may be defined differently to ensure a consistency between the datasetdatasets.

620

6 Conclusions

We present a new workflow to process for processing DEM time series of high temporal resolution that is specifically designed to preserve the elevation signal of glacier surge events. We applied the workflow to a dataset from the ASTER sensor over 630 2000-2019. We filter the data with a LOWESS algorithm, which preserves the surge signal. Some filter issues can appear in difficult areas, which are often not located in surge-affected areas (e.g. textureless accumulation areas, steep slopes). The elevation interpolation (B-spline method ALPS-REML) allows for the observation of surge dynamics, and the estimate of mass transfers at a few months interval. Some surge events covered by only a small number of DEMs can monthly interval. Surge 635 events with too few DEM observations tend to be smoothed, resulting in an underestimation of the surface elevation change and surge duration. Over In our study area in the Karakoram range (HMA), our method provides interpolated time series for 80% of the pixels belonging to glacier areaglacier pixels. Our workflow is able to preserve surge events in a better way than the original non-specific better preserves surge events compared to the original non surge-specific workflow. The resulting data compares fairly well with data obtained are fairly comparable to those from independent studies on several events, except in 640 a few cases. We have discrepancies in estimated volume transferred find discrepancies in the estimated transferred volumes compared to previous studies ranging from 2% to 19% on two surge events and four volumes transferred, and 64% on the Khurdopin surge. It creates a unique dataset The workflow, applied to the ASTER dataset, can generate a unique elevation time series able to represent thickness changes of surge events at a monthly scale over a regional extent. It opens new possibilities for the combined analysis of surges with elevation and velocity datasets, or to follow the evolution of change 645 during surge events, or more complex derivatives such as surface slope and more complex variables driving stress.

Code and data availability. Although the study of Shekhar et al. (2021) only describes the ALPS-GCV implementation, the code provided with that study in the repository Shekhar (2020) also contains the implementation of ALPS-REML, which was used without changes in our study. The code of our workflow can be found at the following repository: https://doi.org/10.5281/zenodo.14045604 (Beraud et al., 2024). Sample data of elevation change and surge-affected areas for the four selected glaciers are also available in that repository.

650 7 Additional time series

655

Additional time series complementing the figure Fig. 6, at coordinates (36.126, 75.158) over the Hispar glacier. Additional time series. Panels a-e show more examples of ALPS-REML interpolation with distinct flaws. The panel d compares the interpolation results of Hugonnet et al. (2021) ("Original interpolation" and its confidence interval) and this study ("ALPS interpolation" and its t-interval). The panel e show the successive iteration of the LOWESS regression, with points coloured by their estimated error (weight of the regression).

7 Volume transferred on original ASTER data

Date start Date end Imbalance 2014-01 2016-09 -1593 x 10^6 m³ 1123 x 10^6 m³ 2003-07 2007-01 -38 x 10^6 m³ 34 x 10^6 m³ 2016-03 2019-03 -587 x 10^6 m³ 451 x 10^6 m³ 2012-11 2017-01 -191 x 10^6 m³ 199 x 10^6 m³ Volume transferred of surges for the four selected glaciers this time according to the original interpolated ASTER dataset from Hugonnet et al. (2021), during the same period as in the table 1.

7 Volume transferred and mass balance comparison

660

665

670

Individual representation of Fig. 13, elevation change comparison histogram per surge. Each surge is the single one occurring during our study period on the glacier designated, except for Yazghil glacier for which the surge is the 2003-2007 one. Note that the reservoir area of the unnamed glacier (RGI code RGI2000-v7.0-G-14-12226) is captured over only a third of its extent here. Comparison of mean elevation change (dh in the figure) per glacier from 2005 to 2015, between the interpolated dataset of Hugonnet et al. (2021) and this workflow. It is calculated over the same valid pixels to avoid different data gaps. It represents 224 glaciers in the center of Karakoram, with 112 glaciers in each surge and non-surge type category. We extract surge-type glaciers from the inventories of Guillet et al. (2022) and Guo et al. (2022) (categories I and II during 2000-2020). The top right histogram represents the difference of mean dh between the two datasets. The dotted lines represent the median of the distributions. The sigma symbol represents the standard deviation.

Author contributions. Luc Beraud: Conceptualization, Methodology, Software, Writing - Original Draft. Fanny Brun and Amaury Dehecq: Conceptualization, Methodology, Writing - Review & Editing, Supervision. Romain Hugonnet and Prashant Shekhar: Software, Writing - Review & Editing.

Competing interests. The authors declare no competing interest.

Acknowledgements. We are grateful to Laurane Charrier for her suggestions and methodological input, and to Adrien Gilbert for our discussions about surge case studies. We thank Etienne Berthier (CNRS, LEGOS) for providing SPOT DEMs and discussing the methodology of the work. We thank also also thank Jakob Steiner for our discussion and his input discussions and additional details related to his published work. We finally thank the French program "Programme National de Télédétection Spatiale (PNTS)" for its funding support.

References

700

- Beaud, F., Aati, S., Delaney, I., Adhikari, S., and Avouac, J.-P.: Surge dynamics of Shisper Glacier revealed by time-series correlation of optical satellite images and their utility to substantiate a generalized sliding law, The Cryosphere, 16, 3123–3148, https://doi.org/10.5194/tc-16-3123-2022, 2022.
 - Benn, D. I., Hewitt, I. J., and Luckman, A. J.: Enthalpy balance theory unifies diverse glacier surge behaviour, Annals of Glaciology, pp. 1–7, https://doi.org/10.1017/aog.2023.23, 2023.
- Beraud, L., Brun, F., Dehecq, A., Hugonnet, R., and Shekhar, P.: Data and code for the publication of a surge-specific DEM workflow on ASTER DEMs., https://doi.org/10.5281/zenodo.14045604, 2024.
 - Berthier, E. and Brun, F.: Karakoram geodetic glacier mass balances between 2008 and 2016: persistence of the anomaly and influence of a large rock avalanche on Siachen Glacier, Journal of Glaciology, 65, 494–507, https://doi.org/10.1017/jog.2019.32, 2019.
- Berthier, E., Vincent, C., Magnússon, E., Gunnlaugsson, A. T., Pitte, P., Le Meur, E., Masiokas, M., Ruiz, L., Pálsson, F., Belart, J. M. C., and Wagnon, P.: Glacier topography and elevation changes derived from Pléiades sub-meter stereo images, The Cryosphere, 8, 2275–2291, https://doi.org/10.5194/tc-8-2275-2014, 2014.
 - Berthier, E., Floriciou, D., Gardner, A. S., Gourmelen, N., Jakob, L., Paul, F., Treichler, D., Wouters, B., Belart, J. M. C., Dehecq, A., Dussaillant, I., Hugonnet, R., Kääb, A., Krieger, L., Pálsson, F., and Zemp, M.: Measuring glacier mass changes from space—a review, Reports on Progress in Physics, 86, 036 801, https://doi.org/10.1088/1361-6633/acaf8e, 2023.
- Bhambri, R., Hewitt, K., Kawishwar, P., and Pratap, B.: Surge-type and surge-modified glaciers in the Karakoram, Scientific Reports, 7, 15 391, https://doi.org/10.1038/s41598-017-15473-8, 2017.
 - Bhambri, R., Hewitt, K., Haritashya, U. K., Chand, P., Kumar, A., Verma, A., Tiwari, S. K., and Rai, S. K.: Characteristics of surge-type tributary glaciers, Karakoram, Geomorphology, 403, 108 161, https://doi.org/10.1016/j.geomorph.2022.108161, 2022.
 - Brun, F., Berthier, E., Wagnon, P., Kääb, A., and Treichler, D.: A spatially resolved estimate of High Mountain Asia glacier mass balances from 2000 to 2016. Nature Geoscience. 10, 668–673, https://doi.org/10.1038/ngeo2999, 2017.
 - Burgess, E. W., Forster, R. R., Larsen, C. F., and Braun, M.: Surge dynamics on Bering Glacier, Alaska, in 2008–2011, The Cryosphere, 6, 1251–1262, https://doi.org/10.5194/tc-6-1251-2012, 2012.
 - Charrier, L., Yan, Y., Koeniguer, E. C., Leinss, S., and Trouve, E.: Extraction of Velocity Time Series With an Optimal Temporal Sampling From Displacement Observation Networks, IEEE Transactions on Geoscience and Remote Sensing, 60, 1–10, https://doi.org/10.1109/TGRS.2021.3128289, 2022.
 - Chudley, T. R., Howat, I. M., King, M. D., and MacKie, E. J.: Increased crevassing across accelerating Greenland Ice Sheet margins, Nature Geoscience, 18, 148–153, https://doi.org/10.1038/s41561-024-01636-6, 2025.
 - Cleveland, W. S. and Devlin, S. J.: Locally Weighted Regression: An Approach to Regression Analysis by Local Fitting, Journal of the American Statistical Association, 83, 596–610, https://doi.org/10.1080/01621459.1988.10478639, 1988.
- 710 Cressie, N. A. C., ed.: Statistics for spatial data, Wiley series in probability and mathematical statistics Applied probability and statistics, Wiley, New York, rev. ed edn., ISBN 978-1-119-11515-1 978-1-119-11517-5, 1993.
 - Crompton, J. W., Flowers, G. E., and Stead, D.: Bedrock Fracture Characteristics as a Possible Control on the Distribution of Surge-Type Glaciers, Journal of Geophysical Research: Earth Surface, 123, 853–873, https://doi.org/10.1002/2017JF004505, 2018.
- Cuffey, K. M. and Paterson, W. S. B.: The Physics of Glaciers, Elsevier Science, Burlington, 4th ed edn., ISBN guill, oCLC: 761646843, 2010.

- Derkacheva, A., Mouginot, J., Millan, R., Maier, N., and Gillet-Chaulet, F.: Data Reduction Using Statistical and Regression Approaches for Ice Velocity Derived by Landsat-8, Sentinel-1 and Sentinel-2, Remote Sensing, 12, 1935, https://doi.org/10.3390/rs12121935, 2020.
- Echelmeyer, K., Butterfield, R., and Cuillard, D.: Some Observations on a Recent Surge of Peters Glacier, Alaska, U.S.A., Journal of Glaciology, 33, 341–345, https://doi.org/10.3189/S0022143000008935, 1987.
- 720 European Space Agency and Airbus: Copernicus DEM, https://doi.org/10.5270/ESA-c5d3d65, institution: European Space Agency, 2022.
 - Gao, Y., Wang, J., Liu, S., Yao, X., Qi, M., Liang, P., Xie, F., Mu, J., and Ma, X.: Monitoring dynamics of Kyagar Glacier surge and repeated draining of Ice-dammed lake using multi-source remote sensing, Science of The Total Environment, 928, 172467, https://doi.org/10.1016/j.scitotenv.2024.172467, 2024.
- Gardner, A., Fahnestock, M., and Scambos, T.: MEaSUREs ITS_LIVE Landsat Image-Pair Glacier and Ice Sheet Surface Velocities, Version 1, https://doi.org/10.5067/IMR9D3PEI28U, 2022.
 - Girod, L., Nuth, C., Kääb, A., McNabb, R., and Galland, O.: MMASTER: Improved ASTER DEMs for Elevation Change Monitoring, Remote Sensing, 9, 704, https://doi.org/10.3390/rs9070704, 2017.
 - Guillet, G. and Bolch, T.: Bayesian estimation of glacier surface elevation changes from DEMs, Frontiers in Earth Science, 11, 1076732, https://doi.org/10.3389/feart.2023.1076732, 2023.
- Guillet, G., King, O., Lv, M., Ghuffar, S., Benn, D., Quincey, D., and Bolch, T.: A regionally resolved inventory of High Mountain Asia surge-type glaciers, derived from a multi-factor remote sensing approach, The Cryosphere, 16, 603–623, https://doi.org/10.5194/tc-16-603-2022, 2022.
 - Guo, L., Li, J., Li, Z., Wu, L., Li, X., Hu, J., Li, H., Li, H., Miao, Z., and Li, Z.: The Surge of the Hispar Glacier, Central Karakoram: SAR 3-D Flow Velocity Time Series and Thickness Changes, Journal of Geophysical Research: Solid Earth, 125, https://doi.org/10.1029/2019JB018945, 2020.

- Guo, L., Li, J., Dehecq, A., Li, Z., Li, X., and Zhu, J.: A new inventory of High Mountain Asia surge-type glaciers derived from multiple elevation datasets since the 1970s, preprint, ESSD Ice/Glaciology, https://doi.org/10.5194/essd-2022-238, 2022.
- Herreid, S. and Truffer, M.: Automated detection of unstable glacier flow and a spectrum of speedup behavior in the Alaska Range, Journal of Geophysical Research: Earth Surface, 121, 64–81, https://doi.org/10.1002/2015JF003502, 2016.
- Hugonnet, R., McNabb, R., Berthier, E., Menounos, B., Nuth, C., Girod, L., Farinotti, D., Huss, M., Dussaillant, I., Brun, F., and Kääb, A.: Accelerated global glacier mass loss in the early twenty-first century, Nature, 592, 726–731, https://doi.org/10.1038/s41586-021-03436-z, 2021.
 - Hugonnet, R., Brun, F., Berthier, E., Dehecq, A., Mannerfelt, E. S., Eckert, N., and Farinotti, D.: Uncertainty Analysis of Digital Elevation Models by Spatial Inference From Stable Terrain, IEEE Journal of Selected Topics in Applied Earth Observations and Remote Sensing, 15, 6456–6472, https://doi.org/10.1109/JSTARS.2022.3188922, 2022.
 - Imran, M. and Ahmad, U.: Geospatially analysing the dynamics of the Khurdopin Glacier surge using multispectral and temporal remote sensing and ground observations, Natural Hazards, 108, 847–866, https://doi.org/10.1007/s11069-021-04708-7, 2021.
 - Kotlyakov, V. M., Chernova, L. P., Khromova, T. E., Muraviev, A. Y., Kachalin, A. B., and Tiuflin, A. S.: Unique Surges of Medvezhy Glacier, Doklady Earth Sciences, 483, 1547–1552, https://doi.org/10.1134/S1028334X18120152, 2018.
- 750 Lai, Y.-R. and Wang, L.: Monthly Surface Elevation Changes of the Greenland Ice Sheet From ICESat-1, CryoSat-2, and ICESat-2 Altimetry Missions, IEEE Geoscience and Remote Sensing Letters, 19, 1–5, https://doi.org/10.1109/LGRS.2021.3058956, 2022.

- Li, G., Lv, M., Quincey, D. J., Taylor, L. S., Li, X., Yan, S., Sun, Y., and Guo, H.: Characterizing the surge behaviour and associated ice-dammed lake evolution of the Kyagar Glacier in the Karakoram, Tech. rep., Glaciers/Remote Sensing, https://doi.org/10.5194/tc-2022-253, 2023.
- Lovell, A. M., Carr, J. R., and Stokes, C. R.: Topographic controls on the surging behaviour of Sabche Glacier, Nepal (1967 to 2017), Remote Sensing of Environment, 210, 434–443, https://doi.org/10.1016/j.rse.2018.03.036, 2018.
 - Nolan, A., Kochtitzky, W., Enderlin, E. M., McNabb, R., and Kreutz, K. J.: Kinematics of the exceptionally-short surge cycles of Sít' Kusá (Turner Glacier), Alaska, from 1983 to 2013, Journal of Glaciology, 67, 744–758, https://doi.org/10.1017/jog.2021.29, 2021.
- Paul, F.: Revealing glacier flow and surge dynamics from animated satellite image sequences: examples from the Karakoram, The Cryosphere, 9, 2201–2214, https://doi.org/10.5194/tc-9-2201-2015, 2015.
 - Paul, F., Strozzi, T., Schellenberger, T., and Kääb, A.: The 2015 Surge of Hispar Glacier in the Karakoram, Remote Sensing, 9, 888, https://doi.org/10.3390/rs9090888, 2017.
 - Paul, F., Piermattei, L., Treichler, D., Gilbert, L., Girod, L., Kääb, A., Libert, L., Nagler, T., Strozzi, T., and Wuite, J.: Three different glacier surges at a spot: what satellites observe and what not, The Cryosphere, 16, 2505–2526, https://doi.org/10.5194/tc-16-2505-2022, 2022.
- 765 Pu, S.: Optimizing Gaussian processes: Powerful kernels and efficiency improvements, p. 030009, Shanghai, China, https://doi.org/10.1063/5.0222476, 2024.
 - Quincey, D. J., Braun, M., Glasser, N. F., Bishop, M. P., Hewitt, K., and Luckman, A.: Karakoram glacier surge dynamics: KARAKORAM GLACIER SURGE DYNAMICS, Geophysical Research Letters, 38, n/a–n/a, https://doi.org/10.1029/2011GL049004, 2011.
- Rashid, I., Abdullah, T., Glasser, N. F., Naz, H., and Romshoo, S. A.: Surge of Hispar Glacier, Pakistan, between 2013 and 2017 detected from remote sensing observations, Geomorphology, 303, 410–416, https://doi.org/10.1016/j.geomorph.2017.12.018, 2018.
 - Rasmussen, C. E. and Williams, C. K. I.: Gaussian Processes for Machine Learning, The MIT Press, ISBN 978-0-262-25683-4, https://doi.org/10.7551/mitpress/3206.001.0001, 2005.
 - Rizzoli, P., Martone, M., Gonzalez, C., Wecklich, C., Borla Tridon, D., Bräutigam, B., Bachmann, M., Schulze, D., Fritz, T., Huber, M., Wessel, B., Krieger, G., Zink, M., and Moreira, A.: Generation and performance assessment of the global TanDEM-X digital elevation model, ISPRS Journal of Photogrammetry and Remote Sensing, 132, 119–139, https://doi.org/10.1016/j.isprsjprs.2017.08.008, 2017.
 - Round, V., Leinss, S., Huss, M., Haemmig, C., and Hajnsek, I.: Surge dynamics and lake outbursts of Kyagar Glacier, Karakoram, The Cryosphere, 11, 723–739, https://doi.org/10.5194/tc-11-723-2017, 2017.
 - Rupnik, E., Daakir, M., and Pierrot Deseilligny, M.: MicMac a free, open-source solution for photogrammetry, Open Geospatial Data, Software and Standards, 2, 14, https://doi.org/10.1186/s40965-017-0027-2, 2017.
- Ruppert, D., Wand, M. P., and Carroll, R. J.: Semiparametric regression, Cambridge series in statistical and probabilistic mathematics, Cambridge Univ. Press, Cambridge, repr edn., ISBN 978-0-521-78050-6 978-0-521-78516-7, 2009.
 - Sevestre, H. and Benn, D. I.: Climatic and geometric controls on the global distribution of surge-type glaciers: implications for a unifying model of surging, Journal of Glaciology, 61, 646–662, https://doi.org/10.3189/2015JoG14J136, 2015.
- Shean, D.: High Mountain Asia 8-meter DEM Mosaics Derived from Optical Imagery, Version 1, https://doi.org/10.5067/KXOVQ9L172S2, 2017.
 - Shean, D. E., Bhushan, S., Montesano, P., Rounce, D. R., Arendt, A., and Osmanoglu, B.: A Systematic, Regional Assessment of High Mountain Asia Glacier Mass Balance, Frontiers in Earth Science, 7, 363, https://doi.org/10.3389/feart.2019.00363, 2020.
 - Shekhar, P.: ALPS code, https://github.com/p-shekhar/ALPS, gitHub repository, 2020.

- Shekhar, P., Csatho, B., Schenk, T., Roberts, C., and Patra, A. K.: ALPS: A Unified Framework for Modeling Time Series of Land Ice

 Changes, IEEE Transactions on Geoscience and Remote Sensing, 59, 6466–6481, https://doi.org/10.1109/TGRS.2020.3027190, 2021.
 - Steiner, J. F., Kraaijenbrink, P. D. A., Jiduc, S. G., and Immerzeel, W. W.: Brief communication: The Khurdopin glacier surge revisited extreme flow velocities and formation of a dammed lake in 2017, The Cryosphere, 12, 95–101, https://doi.org/10.5194/tc-12-95-2018, 2018.
- Sun, M., Zhou, S., Yao, X., Duan, H., and Zhang, Y.: Surging glaciers in High Mountain Asia between 1986 and 2021, preprint, Glacier-795 s/Glaciers, https://doi.org/10.5194/egusphere-2022-765, 2022.
 - Terleth, Y., Van Pelt, W. J. J., Pohjola, V. A., and Pettersson, R.: Complementary Approaches Towards a Universal Model of Glacier Surges, Frontiers in Earth Science, 9, 732 962, https://doi.org/10.3389/feart.2021.732962, 2021.
 - Thøgersen, K., Gilbert, A., Bouchayer, C., and Schuler, T. V.: Glacier Surges Controlled by the Close Interplay Between Subglacial Friction and Drainage, Journal of Geophysical Research: Earth Surface, 129, e2023JF007 441, https://doi.org/10.1029/2023JF007441, 2024.
- Turrin, J., Forster, R. R., Larsen, C., and Sauber, J.: The propagation of a surge front on Bering Glacier, Alaska, 2001–2011, Annals of Glaciology, 54, 221–228, https://doi.org/10.3189/2013AoG63A341, 2013.
 - Vale, A. B., Arnold, N. S., Rees, W. G., and Lea, J. M.: Remote Detection of Surge-Related Glacier Terminus Change across High Mountain Asia, Remote Sensing, 13, 1309, https://doi.org/10.3390/rs13071309, 2021.
 - Wahba, G.: Spline Models for Observational Data, Society for Industrial and Applied Mathematics, ISBN 978-0-89871-244-5 978-1-61197-012-8, https://doi.org/10.1137/1.9781611970128, 1990.

- Wang, D. and Kääb, A.: Modeling Glacier Elevation Change from DEM Time Series, Remote Sensing, 7, 10117–10142, https://doi.org/10.3390/rs70810117, 2015.
- Wang, Q., Yi, S., and Sun, W.: Continuous Estimates of Glacier Mass Balance in High Mountain Asia Based on ICESat-1,2 and GRACE/-GRACE Follow-On Data, Geophysical Research Letters, 48, e2020GL090 954, https://doi.org/10.1029/2020GL090954, 2021.
- Wendt, A., Mayer, C., Lambrecht, A., and Floricioiu, D.: A Glacier Surge of Bivachny Glacier, Pamir Mountains, Observed by a Time Series of High-Resolution Digital Elevation Models and Glacier Velocities, Remote Sensing, 9, 388, https://doi.org/10.3390/rs9040388, 2017.
 - Williams, C. K. I.: Gaussian Processes for Machine Learning, http://www.newton.ac.uk/files/seminar/20070809140015001-150844.pdf, 2007.
- Yao, X., Zhou, S., Sun, M., Duan, H., and Zhang, Y.: Surging Glaciers in High Mountain Asia between 1986 and 2021, Remote Sensing, 15, 4595, https://doi.org/10.3390/rs15184595, 2023.
 - Yue, L., Chao, N., Chen, G., Chen, L., Zhang, B., Sun, R., Zhang, Y., Wang, S., Wang, Z., Li, F., Yu, N., and Ouyang, G.: Reconstructing Continuous Ice Sheet Elevation Changes in the Amundsen Sea Sector During 2003–2021 by Merging Envisat, ICE-Sat, CryoSat-2, and ICESat-2 Multi-Altimeter Observations, Journal of Geophysical Research: Earth Surface, 128, e2022JF007020, https://doi.org/10.1029/2022JF007020, 2023.
- 820 Zhang, Z., Zhao, J., Liu, S., Zhang, Q., Jiang, Z., Xu, Y., and Su, H.: Characterization of Three Surges of the Kyagar Glacier, Karakoram, Remote Sensing, 15, 2113, https://doi.org/10.3390/rs15082113, 2023.